Article

Developmental Cell

A Temporal Window for Signal Activation Dictates the Dimensions of a Nodal Signaling Domain

Graphical Abstract

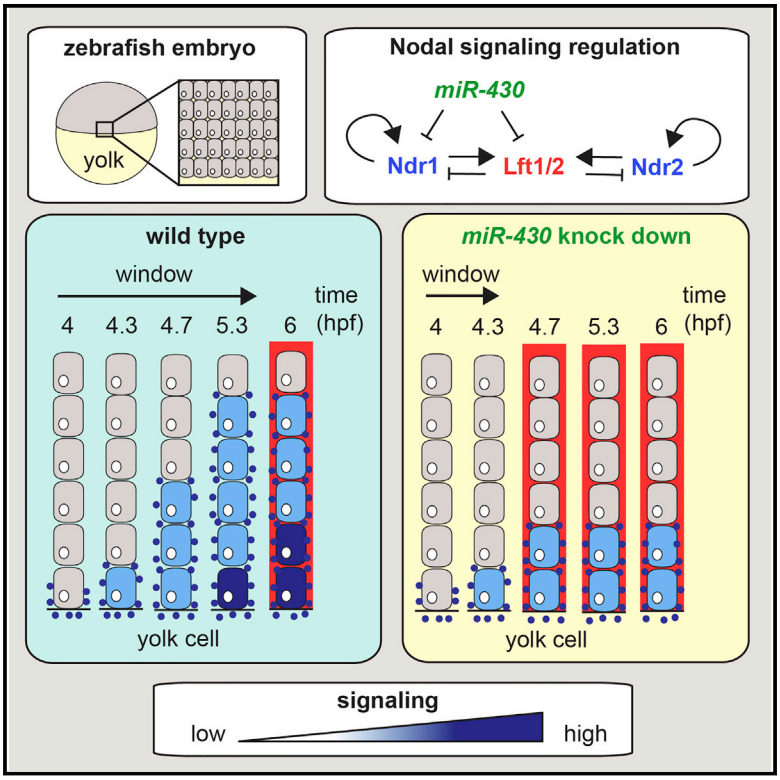

Authors

Antonius L. van Boxtel, John E. Chesebro, Claire Heliot, Marie-Christine Ramel, Richard K. Stone, Caroline S. Hill

Correspondence

caroline.hill@crick.ac.uk

In Brief

van Boxtel et al. show how temporal information in the zebrafish embryo is transformed into a spatial pattern. They demonstrate that the dimensions of the earliest Nodal signaling domain are determined by a temporal signal activation window created by a microRNA-mediated delay in the translation of Lefty, a Nodal antagonist.

Highlights

- Nodal signals exclusively in cells that express both ligand and antagonist
- Lefty1 protein levels are low until the onset of gastrulation
- *miR-430* represses Lefty translation, creating a signal activation window
- Duration of Nodal pathway activation translates into graded signaling

van Boxtel et al., 2015, Developmental Cell *35*, 175–185
October 26, 2015
http://dx.doi.org/10.1016/j.devcel.2015.09.014

CellPress

Developmental Cell
Article

A Temporal Window for Signal Activation Dictates the Dimensions of a Nodal Signaling Domain

Antonius L. van Boxtel,[1] John E. Chesebro,[1] Claire Heliot,[1] Marie-Christine Ramel,[1,3] Richard K. Stone,[2] and Caroline S. Hill[1,*]
[1]Developmental Signalling
[2]Experimental Histopathology
The Francis Crick Institute, Lincoln's Inn Fields Laboratory, 44 Lincoln's Inn Fields, London WC2A 3LY, UK
[3]Present address: Department of Life Sciences, Division of Cell and Molecular Biology, Imperial College London, London SW7 2AZ, UK
*Correspondence: caroline.hill@crick.ac.uk
http://dx.doi.org/10.1016/j.devcel.2015.09.014

SUMMARY

Morphogen signaling is critical for the growth and patterning of tissues in embryos and adults, but how morphogen signaling gradients are generated in tissues remains controversial. The morphogen Nodal was proposed to form a long-range signaling gradient via a reaction-diffusion system, on the basis of differential diffusion rates of Nodal and its antagonist Lefty. Here we use a specific zebrafish Nodal biosensor combined with immunofluorescence for phosphorylated Smad2 to demonstrate that endogenous Nodal is unlikely to diffuse over a long range. Instead, short-range Nodal signaling activation in a temporal window is sufficient to determine the dimensions of the Nodal signaling domain. The size of this temporal window is set by the differentially timed production of Nodal and Lefty, which arises mainly from repression of Lefty translation by the microRNA *miR-430*. Thus, temporal information is transformed into spatial information to define the dimensions of the Nodal signaling domain and, consequently, to specify mesendoderm.

INTRODUCTION

In the development and patterning of embryonic and adult tissues, secreted signaling molecules of the Wnt, Fgf, Hedgehog, and transforming growth factor β (TGF-β) families can act as morphogens to activate different transcriptional programs along a signaling gradient (Perrimon et al., 2012). Ideas of how morphogens impart spatial information have been dominated by the assumption that these molecules form concentration gradients by diffusion, inducing dose-dependent responses in the receiving field of cells. However, it is becoming increasingly clear that for some ligands, for example, Hedgehog, Wnt, and Fgf, other mechanisms, such as short-range signaling activation, transcriptional feedback, and cellular rearrangements, underlie morphogen function (Alexandre et al., 2014; Cohen et al., 2013; Durdu et al., 2014).

Regulation of Nodal signaling in the zebrafish embryo has long served as a paradigm for understanding how morphogens pattern tissues (Schier, 2009). Nodals are secreted ligands that belong to the TGF-β superfamily of growth and differentiation factors. During vertebrate development, Nodal is required for stem cell maintenance, specification of mesoderm and endoderm (mesendoderm), and establishment of left-right asymmetry (Shen, 2007). Recent work has also suggested that Nodal signaling is reactivated in advanced cancers, where it may be important for self-renewal of cancer stem cells (Wakefield and Hill, 2013).

Nodal ligands signal through serine/threonine kinase receptor complexes comprising two type I receptors (Acvr1ba [Taram-a]), two type II receptors (Acvr2a/b), and the co-receptor Tdgf1 (Cripto/Oep) (Schier, 2009; Shen, 2007). Ligand binding activates the receptors, after which the type I receptor phosphorylates the intracellular signal transducers Smad2 and Smad3, which then bind Smad4 (Massagué, 2012). These Smad2/3-Smad4 complexes accumulate in the nucleus, where, together with transcription factors such as Foxh1, Mixer, and Oct4, they regulate gene transcription (Gaarenstroom and Hill, 2014).

At zebrafish blastula stages, two Nodal-related ligands, Ndr1 (Squint) and Ndr2 (Cyclops), specify mesendoderm in marginal cells around the circumference of the embryo by inducing a Smad2-Smad4-Foxh1-dependent transcriptional program (Feldman et al., 1998; Gritsman et al., 1999). Ndr1/2 are thought to form a signaling gradient by diffusion, extending up to about ten cell tiers from the margin (Dubrulle et al., 2015; Harvey and Smith, 2009; Schier, 2009). Indeed, expression of presumed long-range Nodal target genes such as *ta* (*ntla*) and *fscn1a* suggests low-level signaling up to ten cell tiers from the margin (Bennett et al., 2007). This appears supported by bimolecular fluorescent complementation experiments (Harvey and Smith, 2009). However, other Nodal target genes are expressed in up to five to six cell tiers from the margin, which coincides with nuclear accumulation of Smad2-GFP fusion protein (Dubrulle et al., 2015). Importantly, other signaling pathways, such as Bmp, Wnt, and Fgf, are also active at the margin, which can potentially co-regulate Nodal target genes and thus contribute to their expression domains.

Formation of the Nodal signaling domain at the correct time and of appropriate dimensions is thought to be controlled by a reaction-diffusion system (Meinhardt, 2009; Schier, 2009). This model requires positive and negative feedback, which is provided by Nodal-induced expression of both the ligands Ndr1/2 and the antagonists Lefty1 (Lft1) and Lefty2 (Lft2) (Chen and

Shen, 2004; Cheng et al., 2004). Besides these feedback mechanisms, the model requires Lft1/2 to be more diffusible than Ndr1/2 (Müller et al., 2012; Schier and Talbot, 2005). These conditions are thought to allow Ndr1/2 to activate signaling at the margin, whereas Lft1/2 proteins would inhibit signaling in more distal cells. Overexpression studies have shown that Ndr1/2 and Lft1/2 can differentially diffuse and that Ndr1, but not Ndr2, can diffuse over a distance to activate signaling (Chen and Schier, 2001, 2002; Müller et al., 2012). However, the importance of diffusion of endogenous Ndr1/2 remains unclear, as mesendoderm can develop normally in zygotic *ndr1* mutants (Dougan et al., 2003; Feldman et al., 1998; Lim et al., 2013).

In addition to the negative feedback provided by Lft1/2, Nodal signaling is regulated by the *miR-430/427/302* family of microRNAs (miRNAs) (Bassett et al., 2014; Choi et al., 2007; Rosa et al., 2009). At blastula stages, the *miR-430* family is the most abundant family of miRNAs in the zebrafish. Importantly, *miR-430* regulates *ndr1*, *lft1*, and *lft2*, but not *ndr2*, and this is thought to dampen Nodal signaling (Choi et al., 2007). However, to what extent *miR-430*s contribute to the formation of the Nodal signaling domain is unknown.

To develop a specific readout for endogenous Nodal signaling, avoiding overexpression of any pathway components, we generated a transgenic zebrafish Nodal reporter line. Using this line combined with immunofluorescence for phosphorylated Smad2 (P-Smad2), we show that Nodal signals exclusively in cells that express Ndr1/2, up to five to six cell tiers from the margin. This prompted us to revisit the mechanism underlying the formation of the Nodal signaling domain. Our data do not support the reaction-diffusion model, but instead, we propose that Nodal activates signaling in a temporal window that is defined by a *miR-430*-mediated delay of Lft1/2 translation. In this way, temporal information is converted into spatial information in the developing embryo.

RESULTS

Regulation of Presumed Long-Range Nodal Target Gene Expression by Fgf Signaling

The range of activity of the Nodal signaling pathway in the blastula margin has mainly been inferred from the expression of endogenous target genes, such as *fscn1a* and in particular *ta* (*ntla*) (Bennett et al., 2007; Gritsman et al., 1999). However, in addition to Nodal, Fgf signaling is also known to regulate *ta* expression (Griffin et al., 1995; Rodaway et al., 1999; Schier and Talbot, 2005). Genes encoding Fgf ligands, such as *fgf3* and *fgf8a*, are expressed in the margin (Figure S1A) and are known Nodal targets (Mathieu et al., 2004), suggesting that Fgf signaling at the margin of blastula-stage embryos is downstream of Nodal signaling (Rodaway et al., 1999). This is clearly demonstrated by treating embryos with the Nodal inhibitor SB-505124 (Hagos and Dougan, 2007), which results in a near complete loss of phosphorylated Erk (P-Erk), a readout for Fgf pathway activity (Dorey and Amaya, 2010) (Figures 1A and 1B).

Given that both Nodal and Fgf signaling are active at the margin, we examined to what extent Fgf signaling regulates endogenous Nodal target genes, focusing on the expression of *ta* and *fscn1a* as examples of long-range genes and *lft1* and *lft2* as examples of short-range target genes (Bennett et al., 2007; Dubrulle et al., 2015; Harvey and Smith, 2009). To inhibit Fgf signaling, wild-type (WT) embryos were treated with the Fgf receptor (FgfR) inhibitor SU-5402 (Mohammadi et al., 1997) or were injected with mRNA encoding a dominant-negative FgfR (dnFgfR) (Amaya et al., 1991) (Figure 1C). Both treatments resulted in a reduction in the size of the expression domains of *ta* and *fscn1a* in the margin of 40%–50% epiboly embryos, but not of *lft1* or *lft2* (Figure 1D). In fact, *lft2* expression was increased. Similarly, morpholinos (MOs) against *fgf3* and *fgf8*a resulted in a reduction of *ta* expression, but not of *lft1* (Figure S1B). qPCR on SU-5402-treated 50% epiboly embryos confirmed the whole-mount in situ hybridization (WISH) results (Figure 1E), and as expected, inhibition of Nodal signaling by SB-505124 led to reduction in expression of all four genes (Figure 1E). Importantly, FgfR inhibition had no effect on C-terminal phosphorylation of Smad2 (P-Smad2) or overall Smad2 levels, demonstrating that Nodal signaling is not affected by Fgf signaling inhibition (Figure 1F).

To quantitate the effect of inhibiting Fgf signaling on the *ta* expression domain, we performed serial sectioning on *ta*-stained embryos at 40% epiboly. In control embryos, *ta* is expressed in an average of about 10 cell tiers from the margin, whereas expression was reduced to six cell tiers in SU-5402-treated embryos (Figures 1G and 1H). This indicated that *ta* expression beyond six cell tiers was due to Fgf signaling and not directly dependent on Nodal. In support of this idea, injection of increasing doses of *fgf8a* mRNA into a maternal zygotic (MZ) *tdgf1*$^{-/-}$ background confirmed that Nodal signaling is not required for induction of *ta* by Fgf, excluding a requirement for synergism between Nodal and Fgf signaling for *ta* expression beyond six cell tiers (Figure S1C). This was further confirmed by the observation that inhibition of Nodal signaling from the 16-cell stage resulted in the loss of both *ta* and *lft1* expression, but when Nodal signaling was inhibited from dome stage, only *lft1* expression was severely reduced, whereas the expression of *ta* was unaffected (Figure S1D). Thus *ta* expression is not dependent on Nodal activity after Fgf signaling has been initiated.

Together these data demonstrate that Fgf signaling regulates presumed long-range endogenous Nodal target genes beyond six cell tiers.

Direct In Vivo Visualization of Nodal Signaling

To exclusively monitor Nodal signaling without inputs from other pathways, we generated a transgenic zebrafish Nodal reporter line, specific for Smad2-Smad4-Foxh1-mediated signaling. An *eGFP* reporter gene under the control of three Foxh1 and Smad binding sites, termed activin response elements (AREs) (Germain et al., 2000), was inserted into the zebrafish genome using Tol2-mediated transgenesis (*Tg[ARE:eGFP]*) (Figure 2A). We chose this reporter, which we have extensively characterized in a number of cell culture and developmental contexts (Germain et al., 2000; Inman and Hill, 2002; Randall et al., 2004), because Foxh1 is the primary transcription factor required for immediate early Nodal target gene expression (Pogoda et al., 2000; Slagle et al., 2011). In addition, Smad2 is the predominant receptor-regulated Smad during blastula stages (Figure S2A), and indeed MZ deletion of Smad2 results in a phenotype identical to MZ*tdgf1*$^{-/-}$ embryos (Dubrulle et al., 2015).

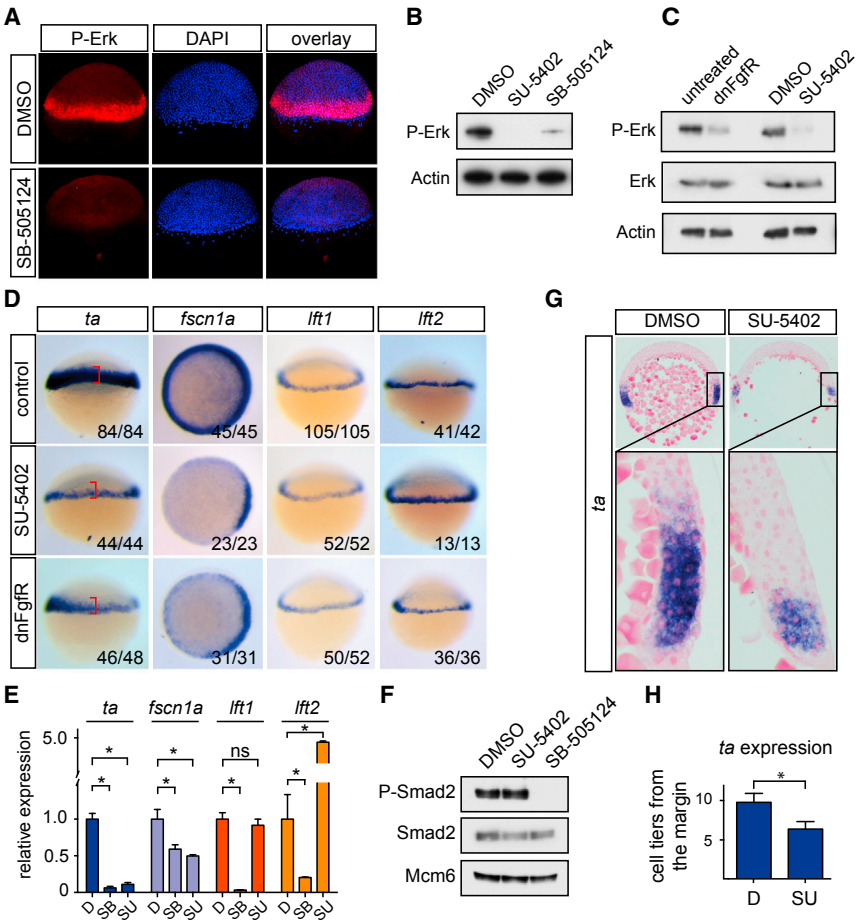

Figure 1. Expression of *ta* and *fscn1a* in the Margin Is Regulated by Fgf Signaling

(A) Whole-mount immunofluorescence for phosphorylated Erk (P-Erk) in DMSO- and SB-505124-treated 50% epiboly embryos. DAPI labels the nuclei.

(B) Western blot for P-Erk in pooled 50% epiboly embryos treated with indicated compounds. Actin is a loading control.

(C) Western blot for P-Erk and total Erk in pooled 40%–50% embryos after control treatment or FgfR inhibition. Actin is a loading control.

(D) WISH for *ta*, *fscn1a*, *lft1*, and *lft2* in control embryos, embryos incubated with SU-5402, or embryos injected with mRNA encoding dnFgfR, at 40%–50% epiboly. For *fscn1a*, animal views are shown. Red brackets outline the width of the WT *ta* expression domain.

(E) qPCR for indicated Nodal target genes on pooled 50% epiboly embryos treated with DMSO (D), SB-505124 (SB), or SU-5402 (SU). Depicted is the mean expression ± SD normalized to *eef1a1l1* levels and compared with levels in DMSO-treated cells (*$p < 0.01$, t test; $n = 3$). ns, not significant.

(F) Western blot for P-Smad2 and Smad2 in pooled 40%–50% embryos treated with the indicated compounds. Mcm6 is a loading control.

(G) Sections of DMSO- and SU-5402-treated 40%–50% epiboly embryos stained for *ta*.

(H) Quantification of the number of cell tiers from the margin that express *ta*. Depicted is the mean ± SD (*$p < 0.01$, Mann-Whitney U test; $n > 50$).

See also Figure S1.

In four independent *Tg(ARE:eGFP)* lines, WISH for *eGFP* mRNA revealed that the reporter was activated in identical domains, excluding any effects caused by different integration sites of the transgene (Figures 2A and S2B). The *eGFP* expression domains correspond to the expression domains of Nodal ligands (Schier, 2009) and include the embryonic margin at blastula stages, axial mesoderm during gastrulation, and the left lateral plate mesoderm during somitogenesis (Figures 2A and S3). Incubation of developing *Tg(ARE:eGFP)* embryos with SB-505124 resulted in a strong reduction of *eGFP* staining (Figure 2B). This was also the case when *foxh1* MOs were injected or when the *Tg(ARE:eGFP)* embryos were bred into a *tdgf1*$^{-/-}$ background (Figure 2B). The *Tg(ARE:eGFP)* reporter is therefore specific for Smad2-Smad4-Foxh1-mediated Nodal signaling during blastula stages.

To confirm the inducibility of the reporter gene, we exposed dissociated cells from *Tg(ARE:eGFP)* blastula-stage embryos to increasing concentrations of recombinant NODAL and measured gene expression by qPCR. *eGFP* expression was induced at identical NODAL concentrations compared with *ta*, suggesting equal sensitivity of the reporter compared with this target gene (Figure 2C). Historically the sensitivity of Nodal target genes, such as *ta* and *noto* (*flh*), has been assessed by ectopically expressing Nodal ligands in the animal pole of blastula-stage embryos and using WISH to assay gene expression (Chen and Schier, 2001). Using NODAL-coated beads in such an assay, we found that the reporter was induced in a domain of similar size to that of *ta* and *noto* (Figure 2D). Finally, we found no differences in the expression of downstream Nodal genes in 40%–50% epiboly embryos by qPCR and WISH when we compared WT and *Tg(ARE:eGFP)* embryos, demonstrating that the introduction of the transgene had no impact on Nodal signaling (Figures S2C–S2E). In conclusion, the *Tg(ARE:eGFP)* zebrafish line is a specific and sensitive biosensor for early Nodal signaling.

Nodal Signaling Is Initiated by Both Maternal and Yolk Syncytial Layer-Derived Ligands

We next used the *Tg(ARE:eGFP)* reporter line to determine how Nodal signaling is initiated in the embryo. At the 8-cell and 1,000-cell stages, no *eGFP* mRNA could be detected (Figure 2E), indicating that *eGFP* mRNA is not maternally contributed. At sphere stage, however, signaling cells are detected as a localized cluster of *eGFP*-positive cells (Figure 2F). From 30% epiboly until the onset of gastrulation, Nodal signaling is detected in the entire margin, with a shallow staining gradient running from dorsal to ventral (Figure 2F). As expected, the overall expression of *eGFP* correlated well with increasing levels of P-Smad2 (Figure 2G).

We compared the spatial and temporal activation of Nodal signaling in *Tg(ARE:eGFP)* embryos with the expression of

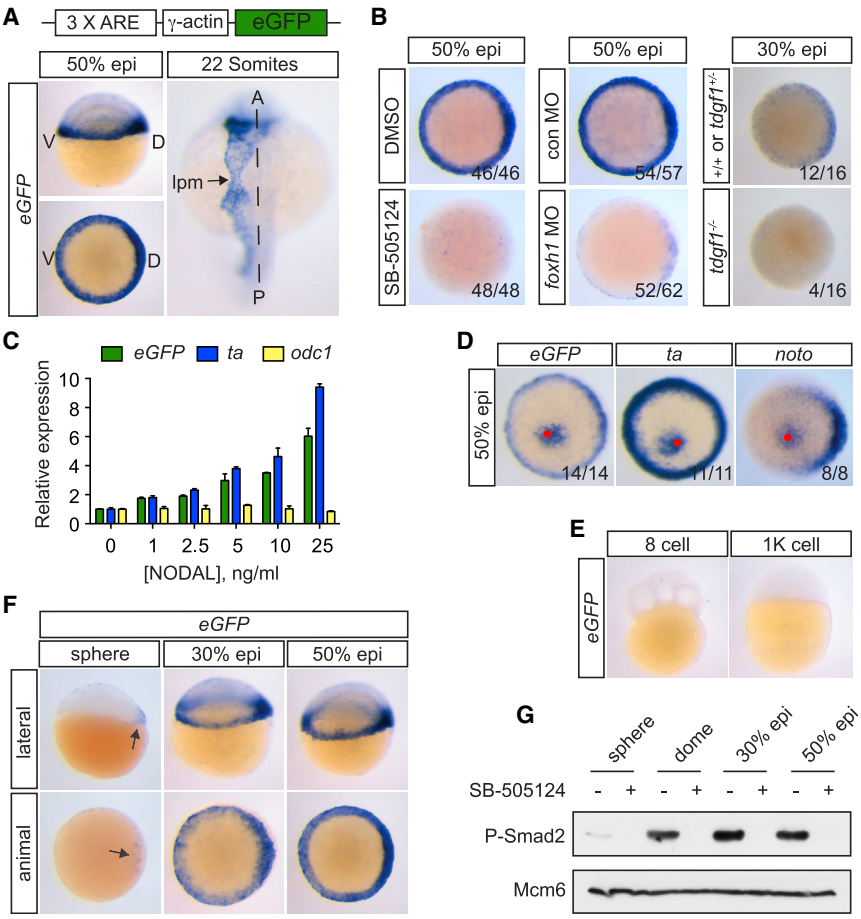

Figure 2. The *Tg(ARE:eGFP)* Zebrafish Line Is a Sensitive and Specific In Vivo Nodal Reporter

(A) Top: schematic representation of the Nodal reporter gene construct. Bottom: WISH for *eGFP* in *Tg(ARE:eGFP)* embryos at 50% epiboly (above, lateral view; below, animal view) and 22 somite stages. Dashed line indicates the midline. A, anterior; D, dorsal; lpm, lateral plate mesoderm; P, posterior; V, ventral.

(B) WISH for *eGFP* in control-treated *Tg(ARE:eGFP)* embryos or after inhibition of Nodal signaling by SB-505124 from the 32-cell stage (left), injection of *foxh1* MO (middle), or in a *tdgf1*$^{-/-}$ background (right) at 50% or 30% epiboly. For the *tdgf1*$^{-/-}$ experiment, a clutch of 16 embryos from a heterozygous incross was analyzed. Note that 25% of embryos lack *eGFP* staining.

(C) qPCR for *eGFP*, *ta*, and *odc1* on dissociated blastula-stage *Tg(ARE:eGFP)* embryonic cells. Depicted is the mean relative expression compared with untreated cells, normalized to *eef1a1l1* levels from one representative experiment ± SD.

(D) Polystyrene beads soaked in recombinant human NODAL were implanted into the animal pole of 1000-cell *Tg(ARE:eGFP)* embryos. Once the embryos had reached ring stage, they were stained for the indicated genes. Animal views are shown. A red spot indicates the position of the bead.

(E) *eGFP* expression at 8-cell and 1,000-cell stages.

(F) *eGFP* expression in sphere, 30% and 50% epiboly *Tg(ARE:eGFP)* embryos. Arrow indicates expression in dorsal cells.

(G) Western blot for phosphorylated Smad2 (P-Smad2) in blastula stage embryos treated with or without SB-505124. Mcm6 is a loading control.

See also Figures S2–S4.

core components of the pathway (Figure S3). The genes encoding the receptor Acvr1ba, the co-receptor Tdgf1, and transcription factors Smad2 and Foxh1 are ubiquitously expressed during blastula stages. The activation of signaling therefore depends exclusively on ligand expression (Figure S3).

The discrete signaling domain at sphere stage likely corresponds to the future dorsal side of the embryo, given the known dorsal localization of maternal *ndr1* mRNA (Figures S3 and S4A) (Gore et al., 2005). We could show that *ndr1* transcripts are polyadenylated before the maternal-to-zygotic transition (Figure S4B), suggesting that maternal *ndr1* is translated and may signal during blastula stages. This was demonstrated by knocking down the Mix-like transcription factor Mxtx2, which is required for zygotic *ndr1* and *ndr2* expression in the yolk syncytial layer (YSL) (Fan et al., 2007; Hong et al., 2011; Xu et al., 2012). *Tg(ARE:eGFP) mxtx2* morphants retained only a small, dorsal domain that expressed *ndr1*, *ndr2*, and *eGFP* (Figure S4C). Loss of the ventrolateral expression of *ndr1/2* in the blastoderm in *mxtx2* morphants suggested that this *ndr1/2* expression was initiated by Nodal ligands secreted by the YSL and resulted from the ability of Ndr1/2 to induce their own expression. Indeed, embryos incubated with the Nodal inhibitor SB-505124 from the 32-cell stage exhibited complete loss of expression of *ndr1/2* in the blastoderm of 40% epiboly embryos, whereas expression of *ndr1/2* in the YSL was not affected (Figure S4D) (Fan et al., 2007).

Thus, maternally provided Ndr1 activates Nodal signaling in dorsal-most embryonic cells before the initiation of signaling in the entire margin by Ndr1/2 synthesized in the YSL (Figure S4E).

Endogenous Nodal Signaling Extends up to Five or Six Cell Tiers from the Margin

The *Tg(ARE:eGFP)* zebrafish line provides an ideal tool to investigate the dimensions of the Nodal signaling domain at the margin. To initially investigate whether there was any Nodal signaling beyond the ligand-expressing domain, we performed double fluorescent WISH for *ndr2* and *eGFP* in 30% epiboly embryos, when the Nodal signaling domain is expanding (Dubrulle et al., 2015; Harvey and Smith, 2009). Although individual signaling cells were occasionally observed directly adjacent to *ndr2*-expressing cells, no *eGFP*-positive cells were detected further beyond the ligand expression domain (Figure S5A). To determine the extent of Nodal signaling more rigorously, 40%–50% epiboly *Tg(ARE:eGFP)* embryos were stained for *eGFP*, *ndr1*, *ndr2*, *lft1*, and *lft2* expression, sectioned, and quantitated (Figures 3A and 3B). The expression of *eGFP*, *ndr1*, *ndr2*, and *lft1* was limited to an average of about five cell tiers, whereas *lft2* expression was detected in only two to three cell tiers from the margin. To confirm that these findings were not due to a lack of sensitivity of the WISH, we analyzed the expression of *sox3*, which is repressed by Nodal signaling in the margin

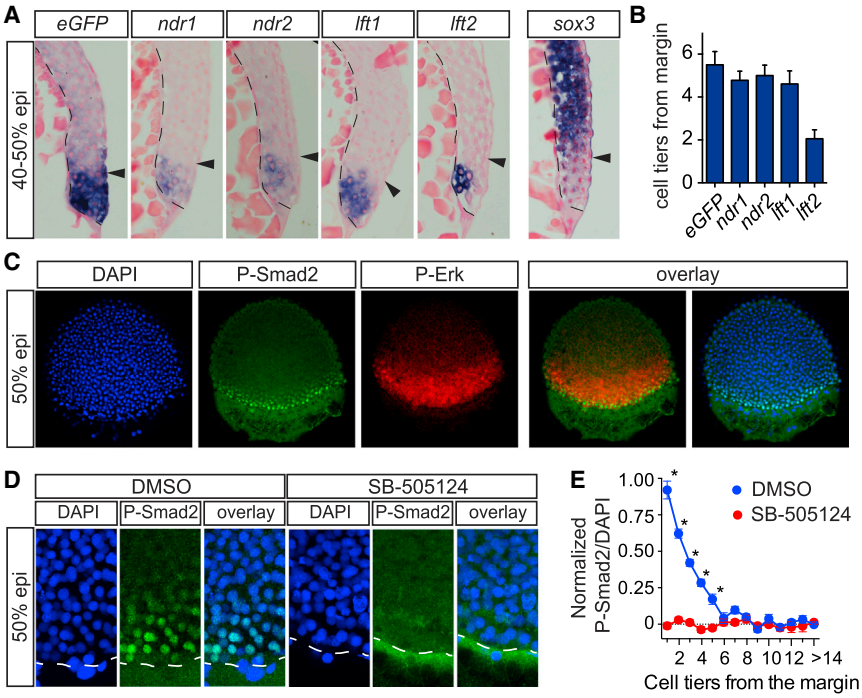

Figure 3. Extent of Nodal Signaling and Target Gene Expression in *Tg(ARE:eGFP)* Embryos

(A) Sections of 40%–50% epiboly embryos, stained for *eGFP*, *ndr1*, *ndr2*, *lft1*, *lft2*, and *sox3*. Sections were counterstained with Nuclear Fast Red. The black line indicates the border of the YSL and blastoderm; arrowheads indicate five cell tiers.

(B) Quantification of the number of cell tiers that express indicated Nodal target genes, calculated from the margin. Depicted is the mean number of cell tiers ± SD (n = 18).

(C) Whole-mount immunofluorescence of 50% epiboly embryos for P-Smad2 and P-Erk. DAPI labels nuclei. Depicted is a single optical slice of a lateral view.

(D) Immunofluorescence for P-Smad2 in DMSO- and SB-505124-treated 50% embryos. Depicted is a Z-projection of a lateral view. The white dashed line indicates the border of the margin.

(E) Quantification of P-Smad2 immunofluorescence normalized to background signal as a function of the number of cell tiers from the margin in DMSO- and SB-505124-treated embryos. Data were binned in 15 μm intervals to represent the average size of a cell in 50% epiboly embryo (Dubrulle et al., 2015). Depicted are means of each bin obtained from multiple optical slices ± SEM (*$p < 0.0$, t test, n = 3, comparing DMSO- and SB-505124-treated intensities for each cell tier).

See also Figure S5.

(Bennett et al., 2007). Significant repression was seen in up to six cell tiers from the margin (Figure 3A). Importantly, staining for all induced Nodal target genes, including *eGFP*, was consistently stronger in a cluster of cells directly proximal to the YSL, where signaling originates (Figure 3A).

To corroborate the data obtained from the sections, we used a direct readout of the Nodal pathway, fluorescent immunostaining of whole-mount 50% epiboly embryos with an antibody against P-Smad2. For comparison, we also stained for P-Erk. Nuclear P-Smad2 staining was observed exclusively in the margin and, as expected, in a smaller domain than the P-Erk staining (Figure 3C). To quantitate the size of the P-Smad2-positive domain, we imaged the embryos at the margin, used MetaMorph software to generate normalized nuclear staining intensities, and measured the distance of each nucleus from the margin in control- and SB-505124-treated embryos. P-Smad2 staining above background was found up to five to six cell tiers (80–90 μm) from the margin in a steep gradient, which was abolished in SB-505124-treated embryos (Figures 3D, 3E, and S5B–S5D). The staining was strongest in the nuclei of cells nearest the YSL. Taken together with our observations from the *Tg(ARE:eGFP)* reporter line, these data demonstrate that Nodal signaling occurs in five to six cell tiers from the margin, closely mirroring the expression of the ligands.

Temporal Regulation of Lft1 Protein Translation during Early Blastula Stages

Our data demonstrate that the Nodal ligands and antagonists are co-expressed at the margin of late blastula-stage embryos, and moreover, Nodal activity is restricted to these cells. This raised two important questions. First, if the ligands and antagonists are co-expressed, how does signaling occur at all? Second, given that all cells are competent to signal at blastula stages and Nodal signaling induces the expression of the ligands, why does signaling not spread throughout the embryo?

To address these questions, we first determined to what extent Lft1/2 regulate Nodal signaling in early and late blastula-stage embryos. The Lft1/2 proteins are known to inhibit signaling by sequestering Tdgf1 and possibly also Nodal itself (Chen and Shen, 2004; Cheng et al., 2004). As expected, injection of *lft1/2* MOs led to an expansion of the Nodal signaling domain at 50% epiboly, which was confirmed by qPCR (Figures 4A and 4B). At dome stage, however, there was no increase in the size of the Nodal signaling domain, suggesting that Lft1/2 do not regulate Nodal signaling at early stages. Although there is an offset in the appearance of *ndr1/2* and *lft1/2* mRNA due to the presence of maternal *ndr1* transcripts, the lack of an early role for Lft1/2 is not explained by an absence of *lft1/2* mRNA at sphere and dome stages (Figures 4C and S3). We hypothesized therefore that a delay in translation of the Lft1/2 proteins could account for the inability of Lft1/2 to regulate Nodal signaling at dome stage. Both *lft1* and *lft2* transcripts were readily polyadenylated by sphere stage (Figure 4D), suggesting that lack of polyadenylation could not account for any delay in Lft1/2 translation.

To measure endogenous protein levels directly, we raised polyclonal antibodies for Lft1 and Lft2 and thoroughly characterized them (Figure S6). Although both antibodies recognized their corresponding target protein when overexpressed (Figure S6B), only the Lft1 antibody was able to detect endogenous protein, so we focused on this family member. The major band detected by

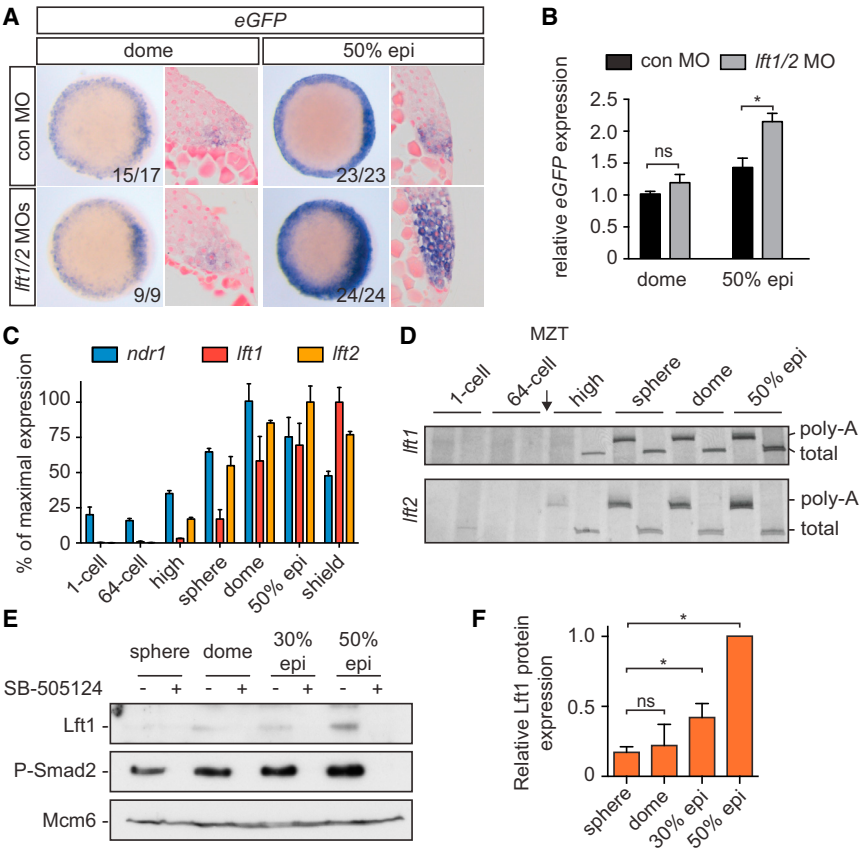

Figure 4. Delayed Translation of Lft1/2 Levels during Early Blastula Stages

(A) WISH for *eGFP* in dome and 50% epiboly *Tg(ARE:eGFP)* embryos, injected with control or *lft1/2* MOs. Animal views are shown at left, and ventrolateral sections are shown at right.

(B) qPCR for *eGFP* mRNA on pooled dome and 50% epiboly embryos. Depicted are means ± SEM (*$p < 0.01$, t test; n = 6).

(C) qPCR for *ndr1*, *lft1*, and *lft2* at different stages. The percentage of mean maximal expression ± SD from a representative experiment performed in triplicate is shown.

(D) Extension poly-A test (ePAT) for *lft1* and *lft2* mRNA. Silver stained non-denaturing polyacrylamide gels are shown indicating total and polyadenylated (poly-A) mRNA.

(E) Western blot showing protein expression of endogenous Lft1 and phosphorylated Smad2 in pooled, blastula-stage embryos. Treatment with SB-505124 is shown to confirm the Lft1 band. Mcm6 is a loading control.

(F) Quantification of Lft1 protein expression from sphere to 50% epiboly. Depicted are the average band intensities of three independent blots, normalized to levels at 50% epiboly ± SD (*$p < 0.05$, t test).

See also Figure S6.

western blot corresponding to endogenous Lft1 migrated by SDS-PAGE with a molecular weight of ~40 kD (Figure S6C). Mutation analysis indicated that this product arose from cleavage at the first Furin cleavage site (marked as C1 in Figure S6A), and we could demonstrate that this product was active (Figures S6D–S6F). The same 40 kD band was also detected in embryos injected with *ndr1* mRNA (Figure S6G). Levels of endogenous Lft1 were barely detectable by western blotting at dome stage and 30% epiboly but increased at 50% epiboly (Figures 4E and 4F). Thus, endogenous Lft1 protein levels remain low until 50% epiboly, despite readily detectable mRNA levels at all these time points. This suggested that the lack of an early role for Lft1/2 could be due to low protein abundance and led us to hypothesize that repressed Lft1/2 translation creates a window of opportunity for Nodal signaling to become established.

miR-430 Creates a Temporal Window for Nodal Signaling by Regulating Lft1/2 Levels

During blastula stages, the *miR-430* family of miRNAs have been reported to block translation, without affecting polyadenylation (Bazzini et al., 2012; Choi et al., 2007). We reasoned therefore that the activity of *miR-430* could be responsible for the repressed translation of Lft1/2 proteins to create a temporal window for Nodal to activate signaling. *miR-430* pri-miRNA is expressed in the nuclei of all cells in the blastoderm, immediately after activation of zygotic transcription (Figure 5A). We also confirmed a ubiquitous expression pattern for mature *miR-430a* and *miR-430b* at 50% epiboly (Figure 5B) and demonstrated that mature *miR-430a* and *miR-430b* are directly processed upon expression (Figure 5C). *miR-430c* was not detected by either WISH or northern blotting, but RNA sequencing data demonstrated that *miR-430c* is much less abundant than *miR-430a* and *miR-430b* (unpublished data). Thus, the *miR-430* family is abundant, ubiquitously expressed, and readily processed during mid to late blastula stages.

To determine the role of *miR-430* in the regulation of Lft1/2 protein translation, we designed three MOs that prevented processing of mature *miR-430a*, *miR-430b*, and *miR-430c*. Injection of these MOs into one-cell-stage embryos resulted in a phenotype resembling MZ *dicer* mutants at 22 hpf (Figure S7A) (Giraldez et al., 2005). Furthermore, they abolished *miR-430a* staining at 50% epiboly and reduced *miR-430a*, *miR-430b*, and *miR-430c* expression, as determined by qPCR, by 89% (Figures S7B and S7C). Co-injection of *miR-430* MOs with a *GFP* reporter containing either three *miR-430* binding sites or a *GFP* reporter with the *lft2* 3′UTR, which contains a single *miR-430* binding site, resulted in increased translation compared to control MOs (Figure S7D). Together, these experiments demonstrate the efficacy of the *miR-430* MOs.

We next injected equal amounts of control or *miR-430* MOs and performed western blotting for P-Smad2 and Lft1 at several blastula stages. In control MO-injected embryos, Lft1 protein was not detectable until 30% epiboly and increased at 50% epiboly, as observed for Lft1 protein expression in WT embryos (compare Figure 4E with Figure 5D). Importantly, this was accompanied by a gradual increase of P-Smad2 over time. In contrast, injection of *miR-430* MOs led to premature translation of Lft1 from dome stage, and this coincided with lower overall

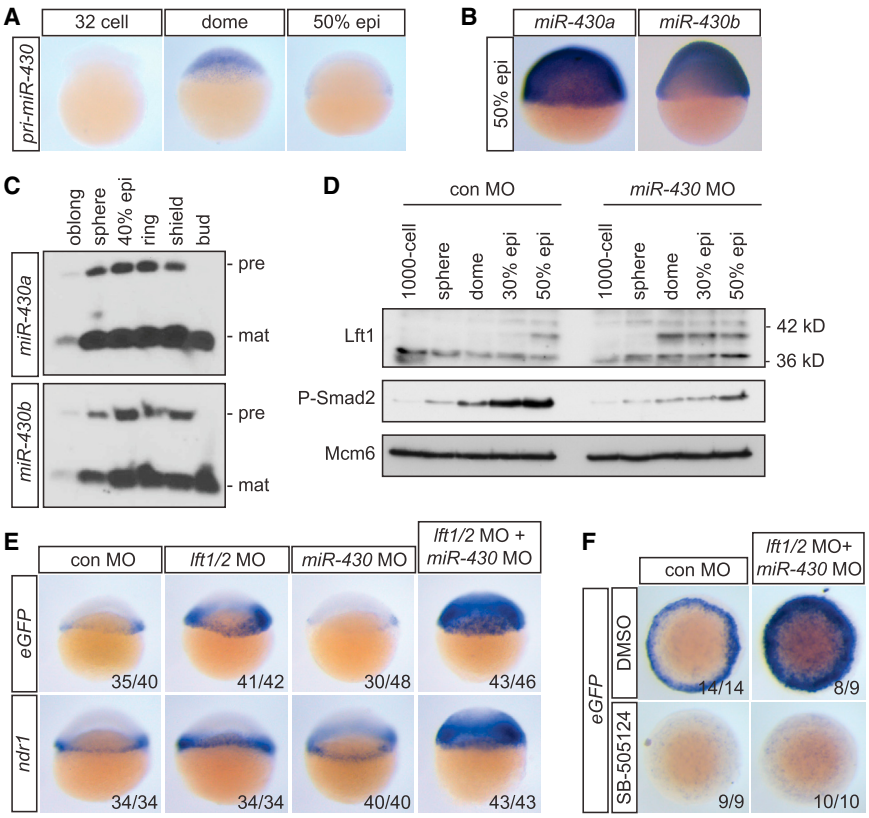

Figure 5. Temporal Regulation of Lft1/2 Translation by *miR-430*s

(A) WISH for *pri-miR-430* at indicated stages.

(B) WISH using LNA probes for mature *miR-430a* and *miR-430b* at 50% epiboly.

(C) Northern blot for *miR-430a* and *miR-430b* at indicated stages using the same probes as in (B). mat, mature miRNA; pre, pre-miRNA.

(D) Western blot for endogenous Lft1 and P-Smad2 in pooled, blastula-stage embryos injected with control or *miR-430* MOs. Mcm6 is a loading control. epi, epiboly.

(E) Lateral views of WISH for *eGFP* reporter and *ndr1* in 30% epiboly, *Tg(ARE:eGFP)* embryos injected with MOs against *lft1/2*, *miR-430* or both.

(F) WISH for eGFP mRNA in 40% epiboly *Tg(ARE:eGFP)* embryos injected with control or combined *lft1/2* and *miR-430* MOs and treated with DMSO or SB-505124. Animal views are shown.

See also Figure S7.

accumulation of P-Smad2 (Figure 5D). Interestingly, the level of Lft1 protein in dome-stage *miR-430* morphants was similar to the maximal level of Lft1 protein measured at 50% epiboly in control MO-injected embryos, suggesting that there may be a threshold level of Lft1 that is inhibitory.

To determine whether reduced signaling in the *miR-430* morphants was due to premature translation of Lft1/2 and to investigate the spatial consequences for Nodal signaling of the loss of *miR-430*, we injected *miR-430* MOs and/or *lft1/2* MOs into *Tg(ARE:eGFP)* embryos and assayed Nodal activity (*eGFP*) and *ndr1* levels at 30% epiboly. Injection of *lft1/2* MOs alone resulted in a modest increase in *eGFP* and *ndr1* staining (Figure 5E), whereas injection of *miR-430* MOs led to a reduction in *eGFP* staining in the blastoderm, consistent with the inhibition of the Nodal signaling pathway we observed using P-Smad2 levels as a readout (Figure 5D). When *lft1/2* MOs and *miR-430* MOs were co-injected, signaling was activated in the entire blastoderm, and this was accompanied by a similar expansion of *ndr1* expression (Figure 5E). Importantly, this spreading of *eGFP* staining in *lft1/2* and *miR-430* MO-co-injected embryos was due to Nodal signaling, because it was completely blocked by incubating double morphants with SB-505124 (Figure 5F). The further spreading of signaling following combined knockdown of *lft1/2* and *miR-430* is readily explained by the regulation of Ndr1 translation by *miR-430* in the absence of Lft1/2 (see Figure 7A) (Choi et al., 2007). Together, these experiments demonstrate that *miR-430* delays Lft1/2 translation to create a temporal window for Nodal to activate signaling.

Duration of Ligand Exposure Translates Directly into Increasing Signaling Levels

Our data demonstrate that a temporal window for Nodal signaling activation determines the size of the Nodal signaling domain and predict that once Lft1/2 levels reach a certain threshold, Nodal signaling is unable to spread to adjacent cells. We therefore tested if blocking signaling activation by recombinant mouse LEFTY1 (mLEFTY1) is dose dependent in dissociated embryonic cells. A 5-fold excess (calculated by mass) of mLEFTY1 over human recombinant NODAL led to a near complete inhibition of signaling activation as read out by western blotting for P-Smad2 and endogenous zebrafish Lft1, which monitors the transcriptional output of the pathway (Figure 6A). Thus, Lft1/2 proteins can reach an inhibitory concentration at which signaling can no longer be activated.

Next we determined if duration of exposure to NODAL directly corresponds to increasing levels of signaling. When blastula-stage cells were exposed to 50 ng/ml NODAL and then inhibited with a blocking concentration of 500 ng/ml mLEFTY1 at different time points, P-Smad2 and endogenous Lft1 levels were indeed proportional to the duration of ligand exposure (Figure 6B).

Finally, we investigated how rapidly signaling is blocked when Lft1/2 levels reach inhibitory concentrations. This is a crucial issue, as we observe that Nodal signaling in vivo (as read out by *eGFP*, *ndr1*, *ndr2*, *lft1*, and *lft2*) is sustained in the margin for several hours after Lft1 levels reach an inhibitory concentration at around 50% epiboly (Figure S3). Dissociated embryonic cells were therefore exposed to NODAL for 1 hr, and then signaling was inhibited by addition of mLEFTY1 for 2 hr. We observed that P-Smad2 levels decreased slowly, compared with the rapid termination of signaling with SB-505124 (Figure 6C). This demonstrated that although signal activation is blocked by Lefty, Nodal signaling is sustained for some time, presumably because of continued signaling from internalized receptor complexes in early endosomes (Jullien and Gurdon, 2005; Vizán et al., 2013).

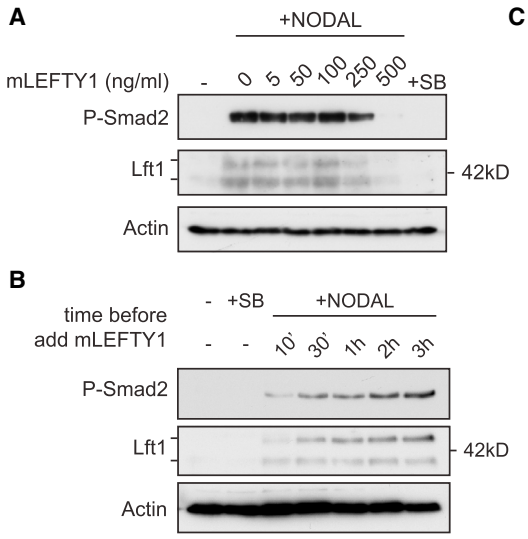

Figure 6. Nodal Signaling Dynamics

(A) Western blot for P-Smad2 and endogenous Lft1 on dissociated blastula-stage embryonic cells. Cells were exposed to 100 ng/ml NODAL for 2 hr, with or without increasing doses of mLEFTY1. Actin is a loading control. Lft1 runs as two bands: the upper one is unprocessed, and the lower is the 40 kD processed band. SB, SB-505124.

(B) Cells were treated ± 10 μM SB-505124 or with 50 ng/ml NODAL and then with 500 ng/ml mLEFTY1 at the indicated time points. All cells were collected at the 3 hr time point and western blotted as indicated.

(C) Top: scheme of the experimental setup. Arrows denote addition of the indicated compound or recombinant protein. All cells were collected at the 3-hr time point. Bottom: western blot using the indicated antibodies. Times (hours) of incubation with 10 μM SB-505124, NODAL, or mLEFTY1 are shown.

In conclusion, our data show that activation of Nodal signaling in blastula-stage cells can occur until Lft1/2 levels reach inhibitory concentrations. Moreover, the levels of P-Smad2, and as a result transcription, are proportional to the duration of signal activation. This can be maintained for some time after inhibitory Lft1/2 concentrations are reached, while no new signaling is activated.

DISCUSSION

A Temporal Window of Signaling Activation Determines the Size and Shape of the Nodal Signaling Domain

Here we describe a specific and sensitive Nodal reporter line that has enabled us to visualize endogenous Nodal signaling in developing zebrafish embryos, without overexpression of any pathway components. We show that signaling is initiated on the dorsal side because of maternally provided Ndr1. Ventral and lateral signaling arises as a result of Ndr1/2 expression in the YSL, which then spreads toward the animal pole as a result of autoregulation. Nodal signaling in the margin reaches a maximum of six cell tiers, which we demonstrate by P-Smad2 immunostaining and reporter activity. We find no evidence of signaling beyond the cells that express the ligand, and moreover, these same cells additionally express the Nodal antagonists Lft1/2. Spreading of presumed long-range Nodal target genes, such as *ta*, that are activated beyond the ligand expression domain, is actually due to Fgf signaling, activated downstream of Nodal. Our data support a model whereby a temporal window for Nodal signaling activation dictates the dimensions of the Nodal signaling domain (Figure 7). Thus, temporal information is translated into spatial information in the developing embryo.

The crucial determinant of the temporal window is the delayed translation of the Lft1/2 proteins, which is mediated by *miR-430*. In addition, maternally provided *ndr1* transcripts and the production of Ndr1/2 by the YSL allow Nodal signaling to be initiated in the blastoderm, before transcription of *lft1/2* (Figure 7C). *ndr1/2* expression in the YSL activates signaling in adjacent cells in the blastoderm. Because of positive feedback, the blastoderm cells produce more Ndr1/2, while Lft1/2 levels remain relatively low because of the ubiquitous synthesis of *miR-430*. In these conditions, Nodal signaling can be activated in neighboring cells until extracellular Lft1/2 levels reach inhibitory concentrations. Therefore, the duration for which Lft1/2 levels are repressed dictates the size of the Nodal signaling domain. How the repressive action of *miR-430* is lifted at 50% epiboly to allow Lft1/2 translation is not yet known and requires further investigation. Although inhibitory Lft1/2 levels prevent further activation of signaling, and hence additional spreading of Nodal signaling, cells already responding to Nodal will continue to signal for several hours, because this occurs from internalized receptors that are refractory to Lft1/2 inhibition. A consequence of our proposed mechanism is that cells directly adjacent to the YSL activate Nodal signaling for the longest duration. This likely explains the more intense P-Smad2 staining in these cells relative to those further from the margin. We therefore propose that Nodal signaling at the margin at blastula stages is dictated by an interplay among ligand, ligand antagonist, and a miRNA, with a differential in timing between ligand and antagonist production being the key determining factor.

The size and shape of the Nodal signaling gradient had previously been thought to be regulated by a reaction-diffusion system (Meinhardt, 2009; Müller et al., 2012; Schier, 2009). Here we propose an alternative mechanism whereby the size of the domain is dictated by the delay in Lefty translation. Although the Nodal/Lefty ligand/antagonist pair has many features of a reaction-diffusion system, we have uncovered one aspect that is incompatible. In reaction-diffusion models, which were originally conceived as pattern-forming chemical reactions, a homogeneous distribution of activator and inhibitor are unstable, and a local elevation of activator initiates formation of a gradient (Meinhardt, 2009). Integral to this model is the ability of the diffusing antagonist to immediately inhibit activator function at a distance. For Nodal and Lefty, this cannot happen, because once Nodal signaling is activated it occurs from internalized receptors and is therefore insensitive to Lefty inhibition, except over prolonged time frames.

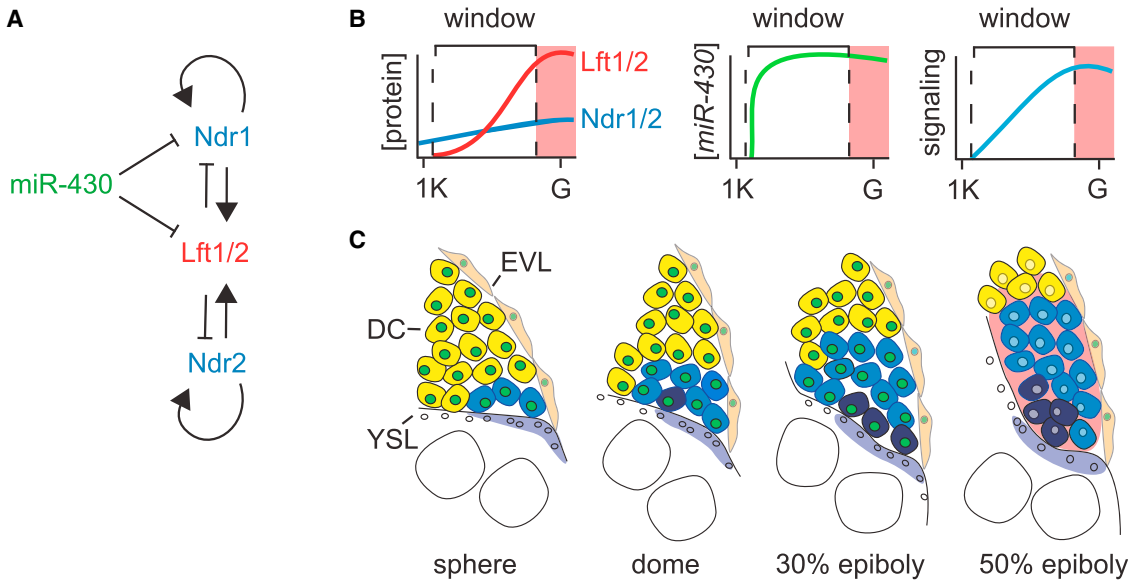

Figure 7. The Nodal Temporal Window Model

(A) Schematic showing how *miR-430*, Lft1/2, and *ndr1/2* regulate one another.

(B) Model of temporal window for Nodal signaling activation, controlled by *miR-430* and Lft1/2. Ndr1/2 protein levels increase (dark blue line) over time because of autoregulation at low Lft1/2 concentrations (red line) until sufficient Lft1/2 is translated to inhibit signaling activation (pink shading) just before the onset of gastrulation. This process is controlled by *miR-430*s (green line, middle), which allows slow accumulation of signaling (light blue line, right). G, gastrulation; 1K, 1,000-cell stage.

(C) In vivo mesendoderm induction over time according to the Nodal temporal window model. YSL-expressing Ndr1/2 is shown in purple; cells responding to Nodal are in blue, with dark blue denoting those experiencing the longest signaling duration. Cells expressing *miR-430* are denoted with green nuclei, and pink shading depicts cells in which Lft1/2 levels have reached an inhibitory threshold. Note that by 50% epiboly the cells beyond the Nodal signaling domain are responding to Fgf, and this accounts for expression of mesodermal genes such as *ta* and *fscn1a* in these cells. For details, see text. DC, deep cells; EVL, enveloping layer.

A Temporal Gradient of Nodal Signaling and Cell Fate Decisions

Our data suggest that spatially graded activity of the Nodal signaling pathway is mainly the result of different durations of exposure to Ndr1/2 over time, as opposed to exposure to different concentrations. We observe two graded signaling domains in *Tg(ARE:eGFP)* embryos that are both explained by timing of ligand exposure. During blastula stages, a shallow signaling gradient runs from dorsal to ventral. This is readily explained by the fact that dorsal cells are exposed to Nodal for a longer period than ventrolateral cells, because maternally provided Ndr1 signals dorsally before Ndr1/2 produced in the YSL induces signaling in the blastoderm margin. In addition, we found a clear vegetal-to-animal gradient within the ligand-expression domain using P-Smad2 immunostaining in late blastula-stage embryos, and we also observed that cells directly adjacent to the YSL expressed higher levels of all Nodal target genes, including the *eGFP* reporter gene, reflecting higher levels of signaling. Again, cells directly adjacent to the YSL are exposed to Ndr1/2 for the longest period of time. The importance of duration of exposure is further supported by our ex vivo experiments with dissociated embryonic cells. The long-term functional consequences of this were demonstrated in previously published work, which linked cell fates to the duration of exposure to Nodal signals (Hagos and Dougan, 2007). Thus, our model explains how concentration and duration of signaling can be translated into positional information. Finally, the importance of timing of signaling activation also rationalizes the normal development of *ndr1* mutants (Feldman et al., 1998; Heisenberg and Nüsslein-Volhard, 1997; Lim et al., 2013). Mesendoderm development in these mutants is largely normal, although delayed. This is explained by the fact that Ndr2 compensates for the lack of Ndr1, but its expression is delayed, because there is no maternal Ndr2.

From the sectioning of *Tg(ARE:eGFP)* embryos and immunostaining for P-Smad2, it is clear that Smad2-Smad4-Foxh1-dependent Nodal signaling is confined to 5–6 cell tiers from the margin, which could imply that all mesendodermal cells arise from this domain. This finding seems to contradict lineage-tracing studies that show that some mesodermal precursors are located up to 12 cell tiers away from the margin (e.g., see Dougan et al., 2003; Warga and Nüsslein-Volhard, 1999). Although these lineage-tracing studies have provided valuable insight into the overall spatial distribution of mesendoderm precursors, they cannot themselves determine the extent of Nodal signaling. This is because although Nodal signaling is required for mesendoderm formation, not all cells that become mesendoderm have necessarily experienced Nodal signaling directly.

Our understanding of how morphogens activate graded signaling in tissues has been dominated by the pre-molecular era assumption that secreted ligands diffuse from a source to form concentration gradients, and this assumption has naturally progressed into the formulation of models that include diffusion as a major determinant in patterning by morphogens. Although in

some contexts, such as the establishment of left-right asymmetry, Nodal can act at long range (Shiratori and Hamada, 2014), the work presented here shows that the formation of the Nodal signaling domain at the blastula margin is explained by short-range signaling activation, signaling dynamics, and transcriptional/translational regulation.

EXPERIMENTAL PROCEDURES

For detailed experimental procedures, see the Supplemental Information.

Recombinant Proteins and Inhibitors

Human NODAL (3218-ND/CF; R&D) was dissolved in 4 mM HCl at 100 μg/ml, aliquoted in non-stick tubes, and used at 40 ng/ml (unless stated otherwise) without freeze-thawing. Recombinant mLEFTY1 was dissolved according to the manufacturer's instructions (994-LF/CF; R&D). The inhibitors SB-505124 (3263; Tocris Bioscience) and SU-5402 (572631; Calbiochem) were dissolved in DMSO and used in embryos at 50 and 10 μM respectively. In dissociated embryonic cells, SB-505124 was used at 10 μM.

Dissociated Embryonic Cell Culture

For blastula-stage cell cultures, up to 1,000 embryos were dechorionated using 2 mg/ml Pronase (11459643001; Roche) in 10 ml E3 medium. The dechorionated embryos were washed extensively in E3 medium and once with calcium-free Ringers buffer to remove the Pronase (Link et al., 2006). The embryos were manually disrupted in calcium-free Ringers buffer using a P200 pipette in 6 cm bacterial dishes, collected by centrifugation at 1,000 × *g* for 5 min, and then resuspended at ~50 embryos/ml in Leibovitz's L15 Medium (11415-064; GIBCO) supplemented with 3% fetal bovine serum (FBS). Cells were plated in 24-well tissue culture plates coated with poly-L lysine (P4707; Sigma) and allowed to attach for 30 min. These experiments were performed at 28°C using pre-warmed buffers in triplicate. The experiments were terminated by aspirating the medium and freezing the plates at −80°C.

Whole-Mount Immunofluorescence and Quantification of P-Smad2 Staining

Embryos were fixed in 4% paraformaldehyde in PBS overnight, dehydrated to 100% methanol, and stored at −20°C until processing. For whole-mount immunofluorescence, embryos were rehydrated to PBS and incubated in cold acetone at −20°C for 20 min. Blocking and antibody incubations were performed in 10% FBS and 1% Triton X-100 in PBS, and washes were performed in PBS/1% Triton. The following primary antibodies were used: α-P-Smad2/3 (8828; Cell Signaling Technology) and α-P-Erk (M8159; Sigma). Note that because of the lack of Smad3 at blastula stages, we solely detect P-Smad2 with the α-P-Smad2/3 antibody. DAPI was used to stain nuclei, and images were acquired on a Zeiss LSM 780 confocal microscope. For quantification of P-Smad2 intensity in deep cells, MetaMorph Software (Molecular Devices) was used to generate P-Smad2 to DAPI ratios from at least three single optical slices per embryo, in three individual DMSO or SB-505124 treated, 50% epiboly embryos. Care was taken not to select mitotic or overlapping nuclei or nuclei from the enveloping layer. To measure the distance of a nucleus to the margin, a line was drawn laterally at the vegetal edge of the margin, and the distance to the nucleus perpendicular to the margin was measured using the MetaMorph Software. To normalize the staining intensity for each embryo, the average ratio of an area further than 11 cell tiers from the margin (>165 μm) was subtracted from each measurement. The data were divided in 15 μm bins, representing the average size of a deep cell at 50% epiboly (unpublished data; Dubrulle et al., 2015). The averages of the binned data for each cell tier, comparing DMSO and SB-505124 treatment, were used for testing for statistical significant differences using paired t tests with a 95% confidence interval.

Animal Experimentation

All the zebrafish work was carried out under a UK Home Office License under the Animals (Scientific Procedures) Act 1986. The license underwent full ethical review and approval by the Cancer Research UK London Research Institute Animal Ethics Committee.

SUPPLEMENTAL INFORMATION

Supplemental Information includes Supplemental Experimental Procedures and seven figures and can be found with this article online at http://dx.doi.org/10.1016/j.devcel.2015.09.014.

AUTHOR CONTRIBUTIONS

A.L.v.B. and C.S.H. conceived the study. A.L.v.B., J.E.C., C.H., and M.-C.R. performed the experiments and analyzed the data with the help of R.K.S. A.L.v.B. and C.S.H. wrote the paper, with input from the other authors.

ACKNOWLEDGMENTS

We would like to thank E. Amaya, A. Giraldez, M. Hammerschmidt, S. Harvey, A. Meng, P. Müller, A. Lekven, S. Reichert, A. Schier, and S. Wilson for reagents. We are very grateful to D. Martin, C. Sergeant, and P. Taylor for fish maintenance, and we also thank the Francis Crick Institute Light Microscopy Facility and Equipment Park. We thank S. Horswell and M. Schaafsma for assistance with statistics. We thank members of the Hill lab, A. Economou, N. Tapon, B. Thompson, and J.P. Vincent, for discussions and insightful comments on the manuscript. This work was supported by Cancer Research UK and the European Commission Network of Excellence EpiGeneSys (HEALTH-F4-2010-257082).

Received: January 13, 2015
Revised: August 11, 2015
Accepted: September 23, 2015
Published: October 26, 2015

REFERENCES

Alexandre, C., Baena-Lopez, A., and Vincent, J.P. (2014). Patterning and growth control by membrane-tethered Wingless. Nature *505*, 180–185.

Amaya, E., Musci, T.J., and Kirschner, M.W. (1991). Expression of a dominant negative mutant of the FGF receptor disrupts mesoderm formation in Xenopus embryos. Cell *66*, 257–270.

Bassett, A.R., Azzam, G., Wheatley, L., Tibbit, C., Rajakumar, T., McGowan, S., Stanger, N., Ewels, P.A., Taylor, S., Ponting, C.P., et al. (2014). Understanding functional miRNA-target interactions in vivo by site-specific genome engineering. Nat. Commun. *5*, 4640.

Bazzini, A.A., Lee, M.T., and Giraldez, A.J. (2012). Ribosome profiling shows that miR-430 reduces translation before causing mRNA decay in zebrafish. Science *336*, 233–237.

Bennett, J.T., Joubin, K., Cheng, S., Aanstad, P., Herwig, R., Clark, M., Lehrach, H., and Schier, A.F. (2007). Nodal signaling activates differentiation genes during zebrafish gastrulation. Dev. Biol. *304*, 525–540.

Chen, Y., and Schier, A.F. (2001). The zebrafish Nodal signal Squint functions as a morphogen. Nature *411*, 607–610.

Chen, Y., and Schier, A.F. (2002). Lefty proteins are long-range inhibitors of squint-mediated nodal signaling. Curr. Biol. *12*, 2124–2128.

Chen, C., and Shen, M.M. (2004). Two modes by which Lefty proteins inhibit nodal signaling. Curr. Biol. *14*, 618–624.

Cheng, S.K., Olale, F., Brivanlou, A.H., and Schier, A.F. (2004). Lefty blocks a subset of TGFβ signals by antagonizing EGF-CFC coreceptors. PLoS Biol. *2*, E30.

Choi, W.Y., Giraldez, A.J., and Schier, A.F. (2007). Target protectors reveal dampening and balancing of Nodal agonist and antagonist by miR-430. Science *318*, 271–274.

Cohen, M., Briscoe, J., and Blassberg, R. (2013). Morphogen interpretation: the transcriptional logic of neural tube patterning. Curr. Opin. Genet. Dev. *23*, 423–428.

Dorey, K., and Amaya, E. (2010). FGF signalling: diverse roles during early vertebrate embryogenesis. Development *137*, 3731–3742.

Dougan, S.T., Warga, R.M., Kane, D.A., Schier, A.F., and Talbot, W.S. (2003). The role of the zebrafish nodal-related genes squint and cyclops in patterning of mesendoderm. Development *130*, 1837–1851.

Dubrulle, J., Jordan, B.M., Akhmetova, L., Farrell, J.A., Kim, S.H., Solnica-Krezel, L., and Schier, A.F. (2015). Response to Nodal morphogen gradient is determined by the kinetics of target gene induction. eLife *4*, e05042.

Durdu, S., Iskar, M., Revenu, C., Schieber, N., Kunze, A., Bork, P., Schwab, Y., and Gilmour, D. (2014). Luminal signalling links cell communication to tissue architecture during organogenesis. Nature *515*, 120–124.

Fan, X., Hagos, E.G., Xu, B., Sias, C., Kawakami, K., Burdine, R.D., and Dougan, S.T. (2007). Nodal signals mediate interactions between the extra-embryonic and embryonic tissues in zebrafish. Dev. Biol. *310*, 363–378.

Feldman, B., Gates, M.A., Egan, E.S., Dougan, S.T., Rennebeck, G., Sirotkin, H.I., Schier, A.F., and Talbot, W.S. (1998). Zebrafish organizer development and germ-layer formation require nodal-related signals. Nature *395*, 181–185.

Gaarenstroom, T., and Hill, C.S. (2014). TGF-β signaling to chromatin: how Smads regulate transcription during self-renewal and differentiation. Semin. Cell Dev. Biol. *32*, 107–118.

Germain, S., Howell, M., Esslemont, G.M., and Hill, C.S. (2000). Homeodomain and winged-helix transcription factors recruit activated Smads to distinct promoter elements via a common Smad interaction motif. Genes Dev. *14*, 435–451.

Giraldez, A.J., Cinalli, R.M., Glasner, M.E., Enright, A.J., Thomson, J.M., Baskerville, S., Hammond, S.M., Bartel, D.P., and Schier, A.F. (2005). MicroRNAs regulate brain morphogenesis in zebrafish. Science *308*, 833–838.

Gore, A.V., Maegawa, S., Cheong, A., Gilligan, P.C., Weinberg, E.S., and Sampath, K. (2005). The zebrafish dorsal axis is apparent at the four-cell stage. Nature *438*, 1030–1035.

Griffin, K., Patient, R., and Holder, N. (1995). Analysis of FGF function in normal and no tail zebrafish embryos reveals separate mechanisms for formation of the trunk and the tail. Development *121*, 2983–2994.

Gritsman, K., Zhang, J., Cheng, S., Heckscher, E., Talbot, W.S., and Schier, A.F. (1999). The EGF-CFC protein one-eyed pinhead is essential for nodal signaling. Cell *97*, 121–132.

Hagos, E.G., and Dougan, S.T. (2007). Time-dependent patterning of the mesoderm and endoderm by Nodal signals in zebrafish. BMC Dev. Biol. *7*, 22.

Harvey, S.A., and Smith, J.C. (2009). Visualisation and quantification of morphogen gradient formation in the zebrafish. PLoS Biol. *7*, e1000101.

Heisenberg, C.P., and Nüsslein-Volhard, C. (1997). The function of silberblick in the positioning of the eye anlage in the zebrafish embryo. Dev. Biol. *184*, 85–94.

Hong, S.K., Jang, M.K., Brown, J.L., McBride, A.A., and Feldman, B. (2011). Embryonic mesoderm and endoderm induction requires the actions of non-embryonic Nodal-related ligands and Mxtx2. Development *138*, 787–795.

Inman, G.J., and Hill, C.S. (2002). Stoichiometry of active smad-transcription factor complexes on DNA. J. Biol. Chem. *277*, 51008–51016.

Jullien, J., and Gurdon, J. (2005). Morphogen gradient interpretation by a regulated trafficking step during ligand-receptor transduction. Genes Dev. *19*, 2682–2694.

Lim, S., Wang, Y., Yu, X., Huang, Y., Featherstone, M.S., and Sampath, K. (2013). A simple strategy for heritable chromosomal deletions in zebrafish via the combinatorial action of targeting nucleases. Genome Biol. *14*, R69.

Link, V., Shevchenko, A., and Heisenberg, C.P. (2006). Proteomics of early zebrafish embryos. BMC Dev. Biol. *6*, 1.

Massagué, J. (2012). TGFβ signalling in context. Nat. Rev. Mol. Cell Biol. *13*, 616–630.

Mathieu, J., Griffin, K., Herbomel, P., Dickmeis, T., Strähle, U., Kimelman, D., Rosa, F.M., and Peyriéras, N. (2004). Nodal and Fgf pathways interact through a positive regulatory loop and synergize to maintain mesodermal cell populations. Development *131*, 629–641.

Meinhardt, H. (2009). Models for the generation and interpretation of gradients. Cold Spring Harb. Perspect. Biol. *1*, a001362.

Mohammadi, M., McMahon, G., Sun, L., Tang, C., Hirth, P., Yeh, B.K., Hubbard, S.R., and Schlessinger, J. (1997). Structures of the tyrosine kinase domain of fibroblast growth factor receptor in complex with inhibitors. Science *276*, 955–960.

Müller, P., Rogers, K.W., Jordan, B.M., Lee, J.S., Robson, D., Ramanathan, S., and Schier, A.F. (2012). Differential diffusivity of Nodal and Lefty underlies a reaction-diffusion patterning system. Science *336*, 721–724.

Perrimon, N., Pitsouli, C., and Shilo, B.Z. (2012). Signaling mechanisms controlling cell fate and embryonic patterning. Cold Spring Harb. Perspect. Biol. *4*, a005975.

Pogoda, H.M., Solnica-Krezel, L., Driever, W., and Meyer, D. (2000). The zebrafish forkhead transcription factor FoxH1/Fast1 is a modulator of nodal signaling required for organizer formation. Curr. Biol. *10*, 1041–1049.

Randall, R.A., Howell, M., Page, C.S., Daly, A., Bates, P.A., and Hill, C.S. (2004). Recognition of phosphorylated-Smad2-containing complexes by a novel Smad interaction motif. Mol. Cell. Biol. *24*, 1106–1121.

Rodaway, A., Takeda, H., Koshida, S., Broadbent, J., Price, B., Smith, J.C., Patient, R., and Holder, N. (1999). Induction of the mesendoderm in the zebrafish germ ring by yolk cell-derived TGF-β family signals and discrimination of mesoderm and endoderm by FGF. Development *126*, 3067–3078.

Rosa, A., Spagnoli, F.M., and Brivanlou, A.H. (2009). The miR-430/427/302 family controls mesendodermal fate specification via species-specific target selection. Dev. Cell *16*, 517–527.

Schier, A.F. (2009). Nodal morphogens. Cold Spring Harb. Perspect. Biol. *1*, a003459.

Schier, A.F., and Talbot, W.S. (2005). Molecular genetics of axis formation in zebrafish. Annu. Rev. Genet. *39*, 561–613.

Shen, M.M. (2007). Nodal signaling: developmental roles and regulation. Development *134*, 1023–1034.

Shiratori, H., and Hamada, H. (2014). TGFβ signaling in establishing left-right asymmetry. Semin. Cell Dev. Biol. *32*, 80–84.

Slagle, C.E., Aoki, T., and Burdine, R.D. (2011). Nodal-dependent mesendoderm specification requires the combinatorial activities of FoxH1 and Eomesodermin. PLoS Genet. *7*, e1002072.

Vizán, P., Miller, D.S., Gori, I., Das, D., Schmierer, B., and Hill, C.S. (2013). Controlling long-term signaling: receptor dynamics determine attenuation and refractory behavior of the TGF-β pathway. Sci. Signal. *6*, ra106.

Wakefield, L.M., and Hill, C.S. (2013). Beyond TGFβ: roles of other TGFβ superfamily members in cancer. Nat. Rev. Cancer *13*, 328–341.

Warga, R.M., and Nüsslein-Volhard, C. (1999). Origin and development of the zebrafish endoderm. Development *126*, 827–838.

Xu, C., Fan, Z.P., Müller, P., Fogley, R., DiBiase, A., Trompouki, E., Unternaehrer, J., Xiong, F., Torregroza, I., Evans, T., et al. (2012). Nanog-like regulates endoderm formation through the Mxtx2-Nodal pathway. Dev. Cell *22*, 625–638.

Developmental Cell

Supplemental Information

A Temporal Window for Signal Activation Dictates the Dimensions of a Nodal Signaling Domain

Antonius L. van Boxtel, John E. Chesebro, Claire Heliot, Marie-Christine Ramel, Richard K. Stone, and Caroline S. Hill

Supplemental Figures

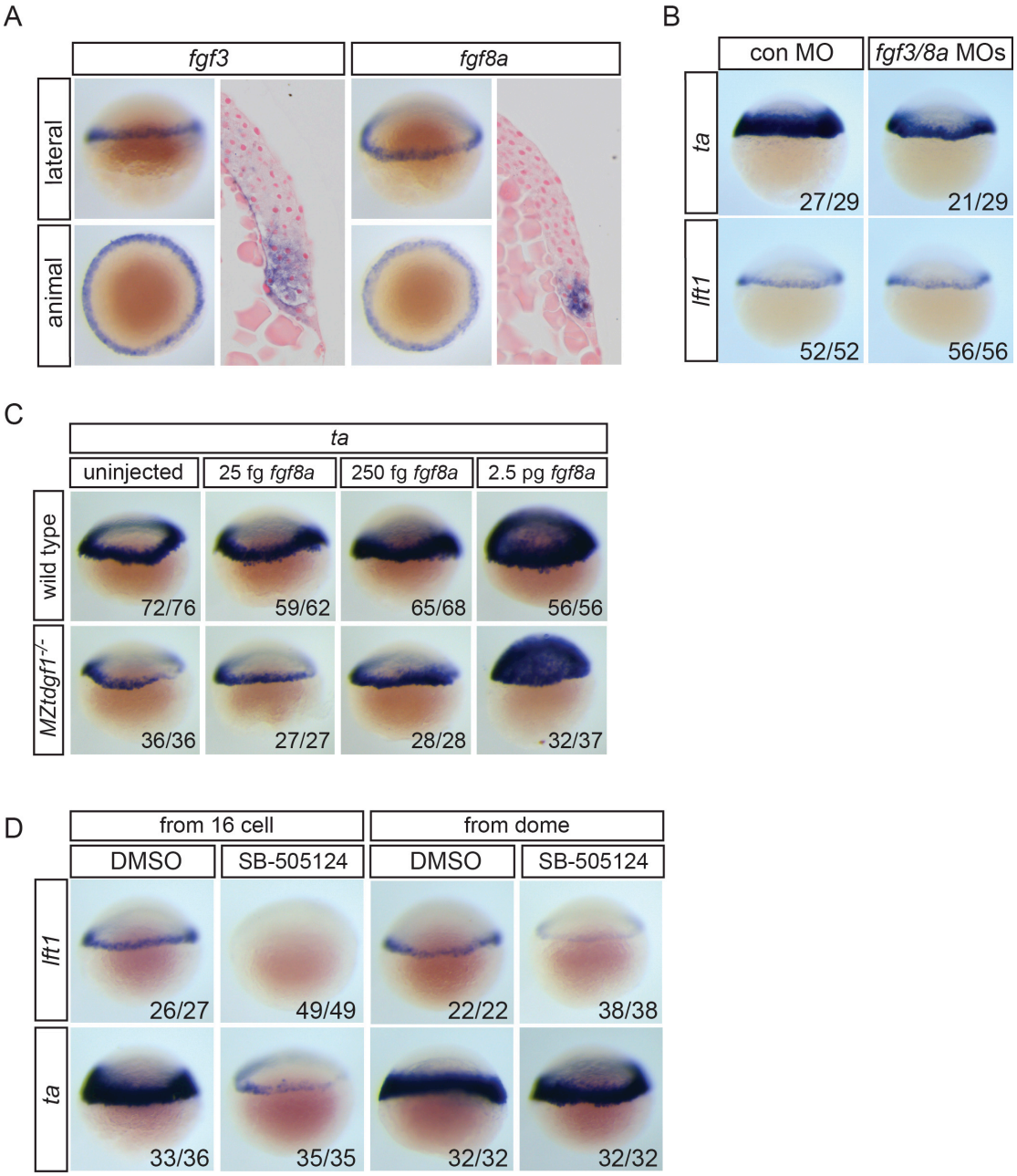

Figure S1, relates to Figure 1. Fgf signaling inhibition and Nodal signaling
(A) Expression of *fgf3* and *fgf8a* in 40% epiboly embryos in the margin shown as WISH and sections.
(B) *ta* and *lft1* expression in 40% epiboly embryos injected with control MO or a combination of *fgf3* and *fgf8a* MOs.
(C) *ta* expression in wild type and maternal-zygotic (MZ) *tdgf1*$^{-/-}$ mutants. *fgf8a* mRNA (25 fg, 250 fg or 2.5 pg) was injected into wild type or MZ*tdgf1*$^{-/-}$ mutant embryos, which were assayed by WISH for *ta* expression at 40% epiboly. *ta* is induced equally well in both backgrounds with 2.5 pg *fgf8a* mRNA.
(D) *lft1* and *ta* expression following inhibition of Nodal signaling with SB-505124 from the 16-cell or dome stage. When inhibited from dome stage, *lft1* expression is severely reduced, whereas *ta* expression is unaffected.

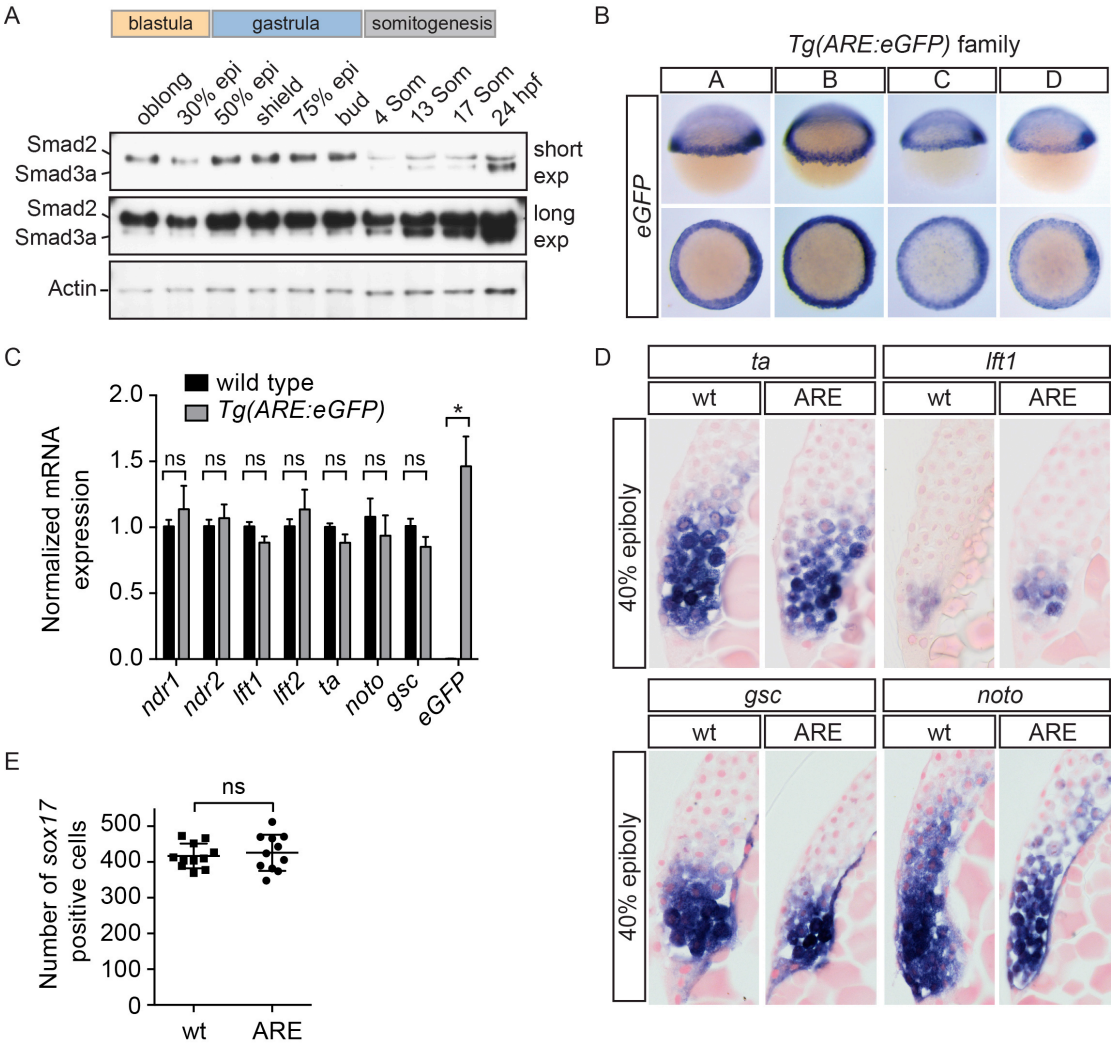

Figure S2, relates to Figure 2. Generation of the *Tg(ARE:eGFP)* transgenic line

(A) Western blot for Smad2 and Smad3a/b during development. Smad3a/b are not expressed at appreciable levels until somitogenesis stages, whereas Smad2 is expressed at all stages shown. A long and short exposure (exp) of the same blot is shown. Actin is a loading control.

(B) WISH for *eGFP* in four *Tg(ARE:eGFP)* lines obtained from independent founders (labeled A–D). Note that individual lines differ slightly in strength of staining and background.

(C) qPCR on pooled 40% epiboly wild type and *Tg(ARE:eGFP)* embryos for the indicated genes normalized to *eef1a1l1*. Means ± SEM are shown (* t-test: $P < 0.05$, n=5). ns, not significant. No significant differences were found for any of the genes tested, except *eGFP*.

(D) Sections of WISH-stained 40% epiboly embryos. No differences were found in the extent of *ta*, *lft1, gsc* or *noto* (*flh*) staining between wild type and *Tg(ARE:eGFP)* embryos. Note that lateral sections are shown for *ta* and *lft1*, whilst dorsal sections are shown for *gsc* and *noto*.

(E) Comparison of the number of *sox17* positive cells in 75% epiboly wild type and *Tg(ARE:eGFP)* embryos. No significant difference was found between the number of endodermal cells between the two lines using a Mann-Whitney U test.

In (D) and (E) wt, wild type; ARE, *Tg(ARE:eGFP)*.

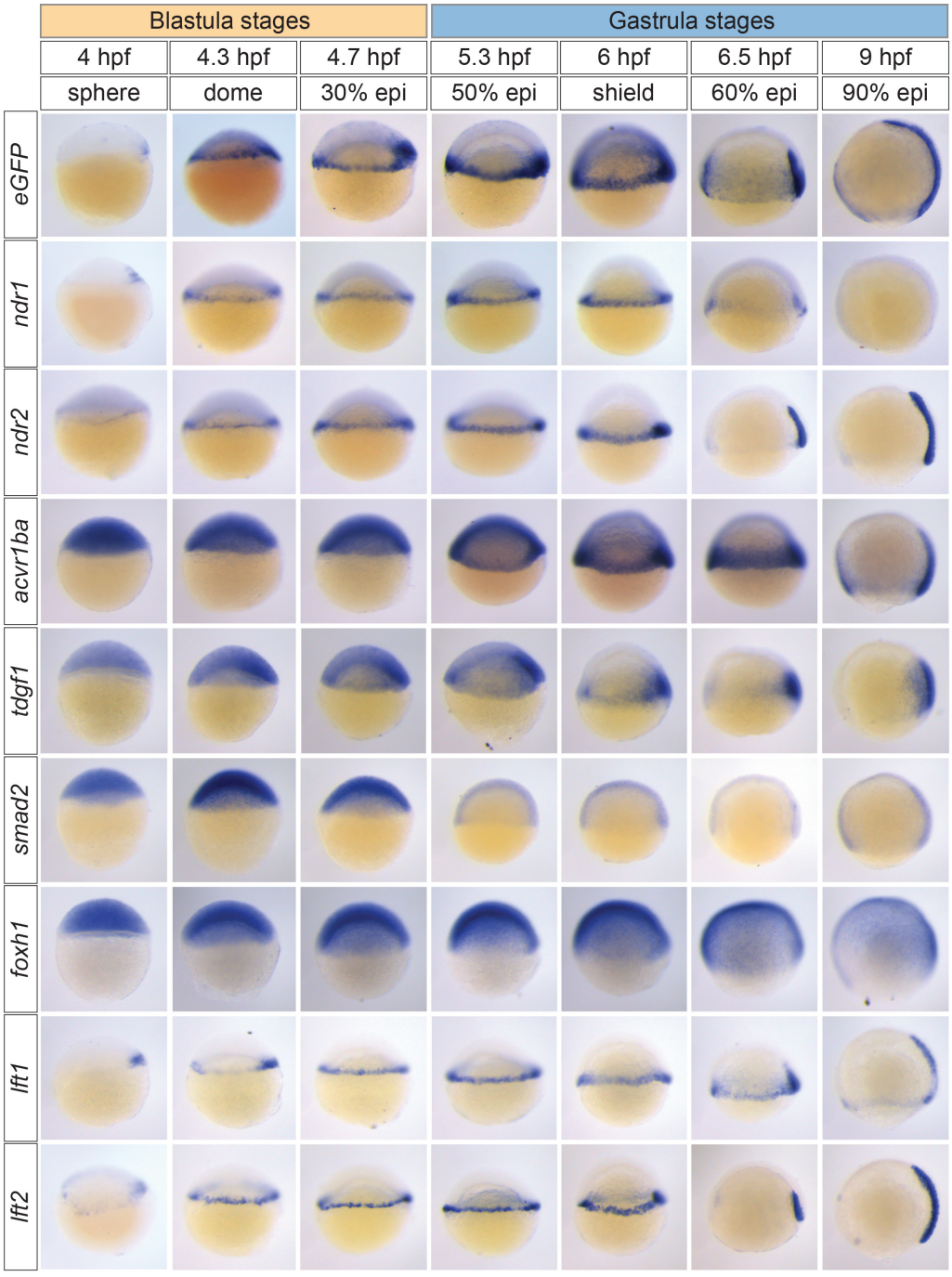

Figure S3, relates to Figure 2. Comparison of Nodal signaling activation in *Tg(ARE:eGFP)* embryos and expression of core components of the Nodal signaling pathway

WISH for *eGFP*, *ndr1* (*sqt*), *ndr2 (cyc)*, *acvr1ba (tar-a)*, *tdgf1 (oep)*, *smad2*, *foxh1 (sur)*, *lft1* and *lft2* in blastula and gastrula stage *Tg(ARE:eGFP)* embryos.

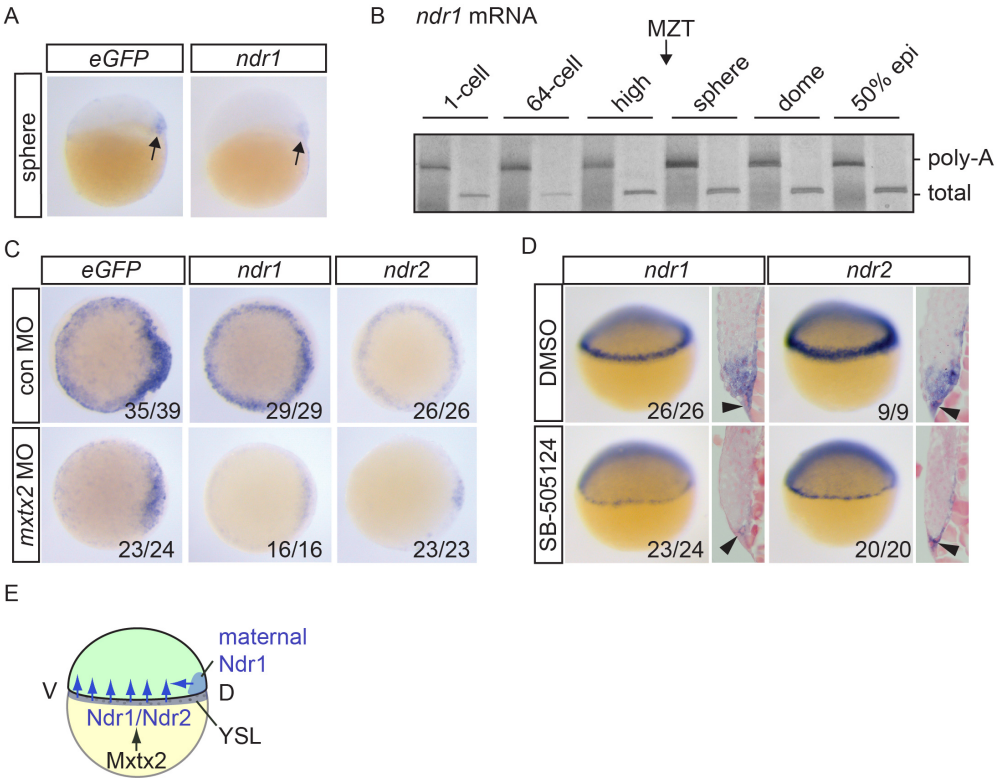

Figure S4, relates to Figure 2. Initiation of Nodal signaling in *Tg(ARE:eGFP)* embryos
(A) *eGFP* and *ndr1* expression in sphere stage embryos. Arrows indicate dorsal expression domains.
(B) ePAT for *ndr1* mRNA. A silver-stained, non-denaturing polyacrylamide gel is shown indicating total and polyadenylated mRNA. Poly-A, polyadenylated; MZT, maternal to zygotic transition.
(C) *eGFP, ndr1* and *ndr2* expression in dome stage *Tg(ARE:eGFP)* embryos injected with control (con) or *mxtx2* MOs. Animal views are shown.
(D) Lateral views and sections of 30-40% epiboly embryos treated with DMSO or SB-505124 at the 32-cell stage and stained for *ndr1* and *ndr2* expression. Black arrowheads indicate expression in the YSL.
(E) Schematic representation showing how Nodal signaling is initiated in zebrafish embryos. For details, see text.

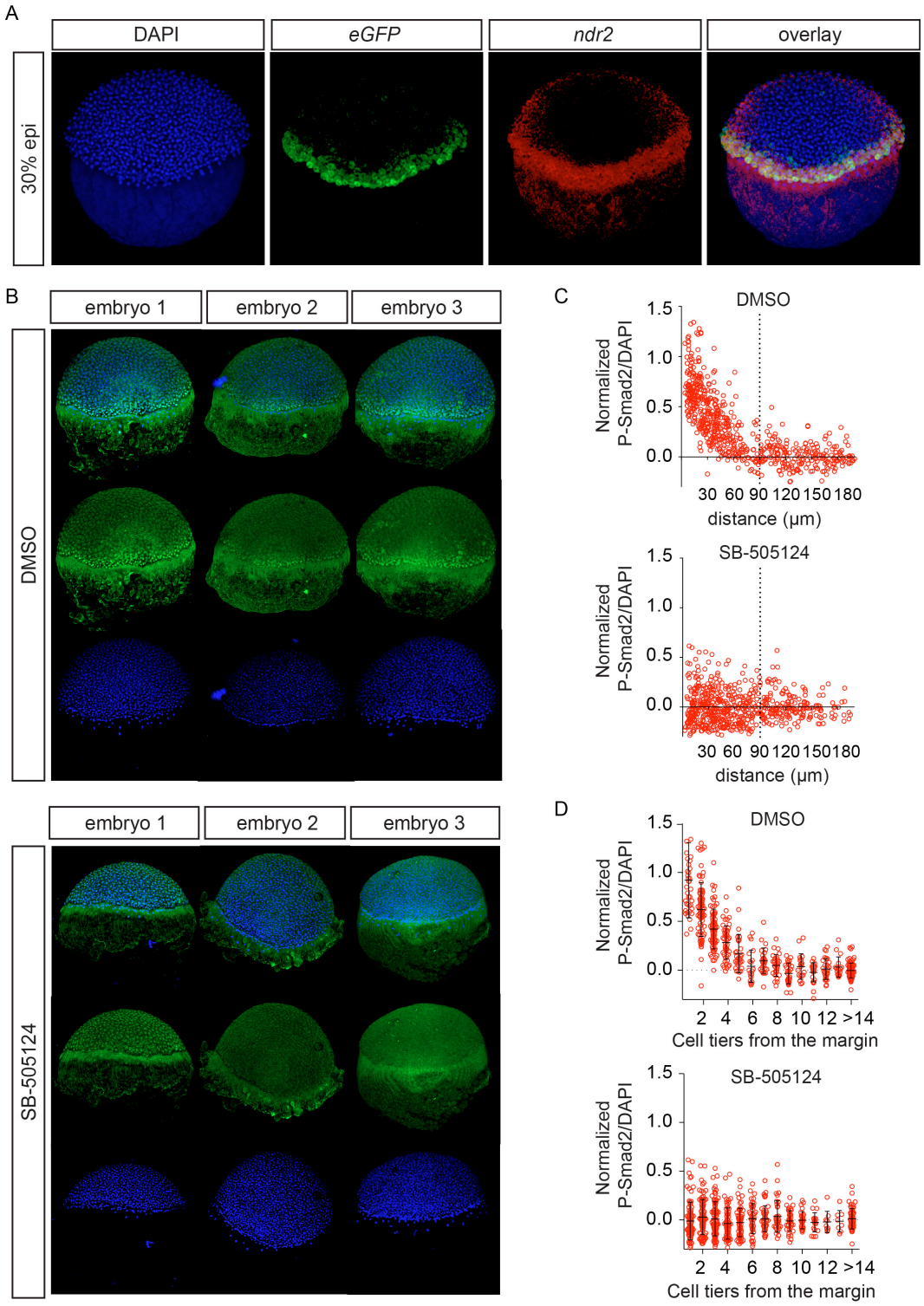

Figure S5, relates to Figure 3. Extent of Nodal signaling in the margin
(A) Double fluorescent WISH for *eGFP* and *ndr2* in 30% epiboly (epi) embryos.
(B) Z-projections of whole mount immunofluorescence for P-Smad2 in 50% epiboly embryos either treated with DMSO or SB-505124, which were used for quantification of Nodal signaling in the margin shown in (C) and (D). DAPI was used as a counter-stain. Note that embryo 3 in both cases are those shown in Figure 1A stained with P-Erk, which was performed as a double whole mount immunofluorescence with the P-Smad2.

(C) Quantification of P-Smad2 staining intensity in DMSO- and SB-505124-treated embryos depicted in (B). Intensities are expressed as P-Smad2/DAPI ratios as a function of distance to the border of the margin. Distance is plotted on the x-axis and the dotted line indicates 90 μm, which corresponds to around six cell tiers.
(D) As in (C) but with data binned in 15 μm bins. The black horizontal line represents the average intensity for each bin ± SD.

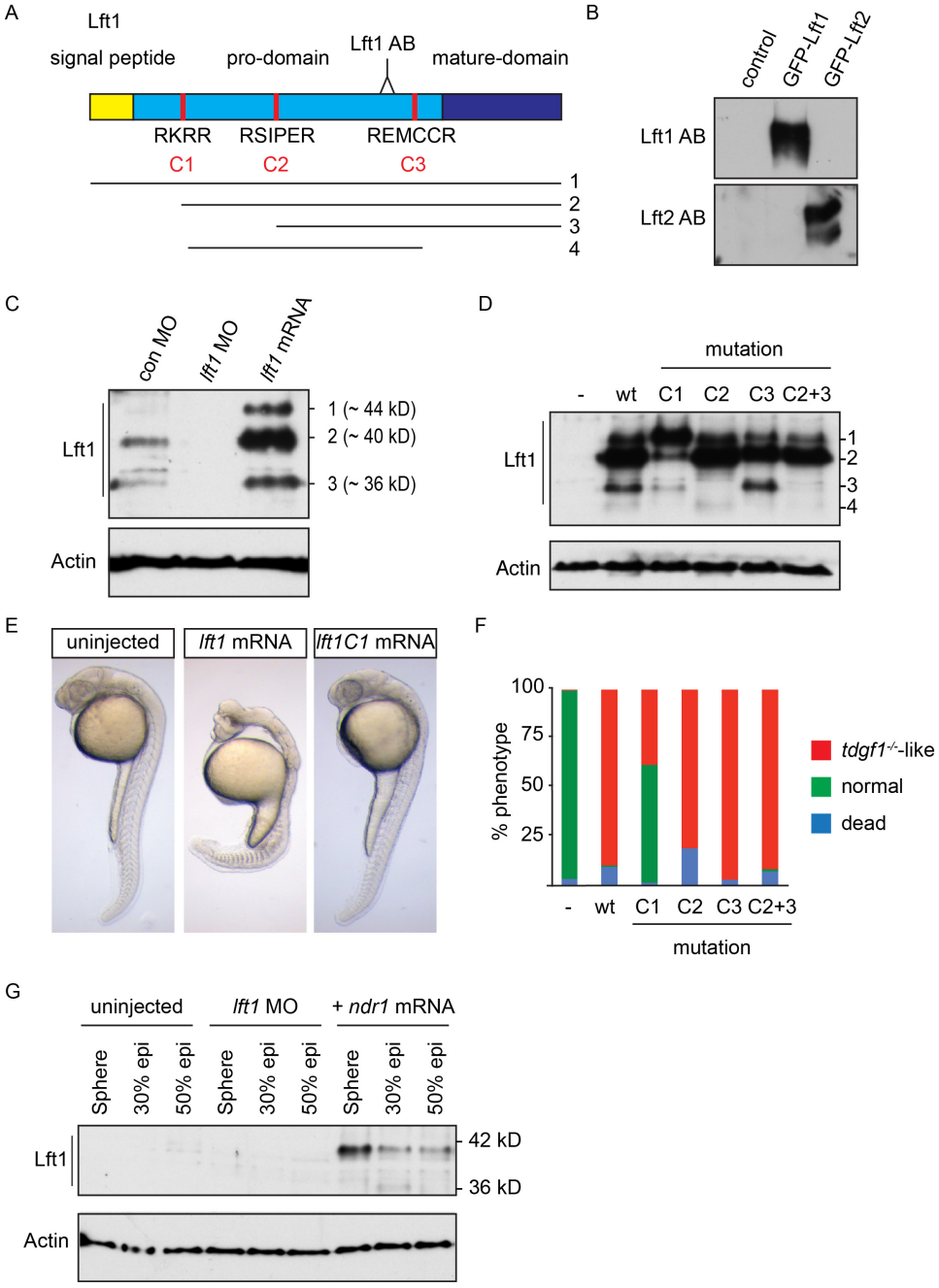

Figure S6, relates to Figure 4. The Lft1 antibody recognizes the 40 kD cleaved and active Lft1 protein

(A) Schematic representation of the zebrafish Lft1 protein. The Lft1 epitope is located in the pro-domain (light blue), just upstream of the mature ligand domain (dark blue). The Lft1 protein contains a signal peptide (gold) and three cleavage sites (C1-C3, red). The cleavage products (1–4) detected by SDS-PAGE are shown. AB, antibody

(B) Western blot for in vitro reticulocyte-translated Lft1 and Lft2 using the cognate antibodies. Note that the Lft1 antibody recognizes GFP-Lft1, but not GFP-Lft2, and vice versa.

(C) Western blot for endogenous and overexpressed Lft1 in pooled 50% epiboly embryo lysates. Overexpressed Lft1 runs as three bands at ~44, ~40, ~36 kD. The second band (~40

kD) corresponds to the main visible endogenous band. These bands are all absent when Lft1 is knocked down using a *lft1* MO.
(D) Western blot for wild type (wt) and mutant overexpressed Lft1 proteins in pooled zebrafish embryos. C1-C3 corresponds to mutated cleavage sites depicted in (A). An additional product (4) is seen in this experiment which results from cleavage at C1 and C3. Actin is a loading control. We conclude that the ~40 kD band arises from cleavage at C1.
(E) Phenotype in 24 hpf wt embryos either uninjected or injected with 5 pg *lft1* or *lft1C1* mutated mRNA. Note that mutating the C1 site leads to rescue of the *lft1* phenotype.
(F) Quantification of phenotypes of 24 hpf embryos, injected with 5 pg wild type or mutant *lft1* mRNAs. Assays were performed on at least 50 embryos.
(G) Western blot for Lft1 in wild type embryos either uninjected or injected with *lft1* MOs or *ndr1* mRNA. Note that both the 40 kD and 36 kD bands are visible in *ndr1*-injected embryos and that the 40 kD band is barely visible in 50% epiboly uninjected embryos.

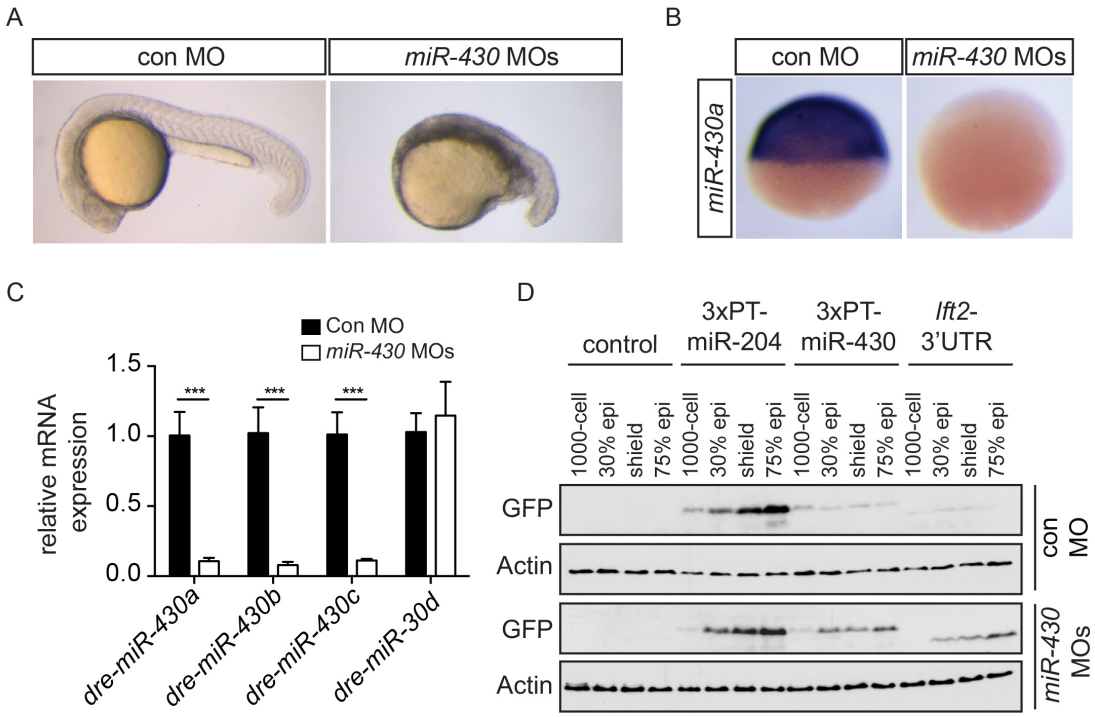

Figure S7, relates to Figure 5. Specificity of the *miR-430* morpholinos
(A) Phenotype of control (con) and *miR-430* morpholino-injected embryos at 22 hpf.
(B) WISH for *miR-430a* with an LNA probe after injection of a mix of *miR-430* or control MOs.
(C) qPCR for *miR-430a*, *b* and *c* after injection of control MOs (black bars) or *miR-430* MOs (white bars). *miR-30d* was not affected by *miR-430* morpholino injection. The data shown are means normalized to control MO ± SD (*** p-value < 0.001, t-test, n=6)
(D) Western blot for GFP on pooled embryo lysates from uninjected embryos or embryos injected with 50 pg mRNA encoding GFP reporter constructs containing 3'UTRs for *miR-204* (3xPT-miR-204), *miR-430* (3xPT-miR-430) or the *lft2* 3'UTR with either control MO or with *miR-430* MOs. *miR-430* MOs lead to an increase in translation of the 3xPT-miR-430 and *lft2*-3'UTR reporter constructs. Note that the GFP in reporters 3xPT-miR-204 and 3xPT-miR-430 migrates more slowly than that in the *lft2* 3'UTR reporter due to a membrane tethering tag. Actin is a loading control.

Supplemental Experimental Procedures

Fish husbandry, transgenesis and staging of embryos

Wild type, *tdgf1*^{tz257}, and *Tg(ARE:eGFP)* zebrafish lines were maintained as previously described (Westerfield, 2000). The *Tg(ARE:eGFP)* transgenic lines were generated by injecting one-cell stage embryos with 60 pg pT2KXGΔin-AREγActin-eGFP plasmid and 50 pg capped *Tol2* transposase mRNA (Kawakami, 2007). Founders for the AREγActin-eGFP transgene were identified by outcrossing injected adult zebrafish to wild type and screening their progeny for *eGFP* expression in the heart at 30 hpf by fluorescence. Fish from eight different founders were raised. Experiments described here use progeny from four different founders. All embryos were carefully staged according to morphological features (Kimmel et al., 1995) to avoid effects caused by general delays in development. In all figures where embryos were manipulated, numbers of embryos showing the representative phenotype out of the total number of embryos assayed are given.

Bead implantations

Bead implantations were performed as previously described with modifications (Picker et al., 2009). Polybead polystyrene 45 μm microspheres (Polysciences, 07314) were washed in ethanol, dried at 50°C and resuspended in 10 μl 100 μg/ml NODAL and incubated for 2 hrs at room temperature. *Tg(ARE:eGFP)* embryos were dechorionated with forceps and individually mounted on 2% agarose injection plates in E3 medium (5.0 mM NaCl, 0.17 mM KCl, 0.33 mM $CaCl_2$, 0.33 mM $MgSO_4$). At the 1000-cell stage, beads were inserted into the blastoderm using a blunt needle and embryos were allowed to develop up to ring stage before fixing in 4% paraformaldehyde (PFA).

Morpholino injections

Morpholinos (MOs) (Gene Tools LLC) were diluted in water and injected at the 1-2 cell stage at concentrations ranging from 2 to 6 ng (Ramel and Hill, 2013). The following MOs were used:

lefty1: 5' - GAAGTCATCTTTTCAAGGTGCAGGA - 3' (Agathon et al., 2001); *lefty2*: 5' - AGCTGGATGAACAGAGCCAT - 3' (Agathon et al., 2001);

foxh1: 5' - TGCTTTGTCATGCTGATGTAGTGGG - 3' (Pei et al., 2007);

mxtx2: 5'- CATTGAGTATTTTGCAGCTCTCTTG - 3' (Bruce et al., 2005);

fgf3: 5'- CATTGTGGCATGGCGGGATGTCGGC - 3' (Maves et al., 2002);

fgf8a: 5'- GAGTCTCATGTTTATAGCCTCAGTA - 3' (Kawakami et al., 2005);

dre-miR-430a: 5'- ACTACCCCAACAAATAGCACTTACC - 3';

dre-miR-430b: 5'- TCTACCCCAACTTGATAGCACTTTC - 3';

dre-miR-430c: 5'- ACTACCCCAAAGAGAAGCACTTATG - 3';

control MO: 5'- CCTCTTACCTCAGTTACAATTTATA - 3'.

Plasmids and mRNA Generation

All oligonucleotides used for cloning are listed in the Table below. To generate the pT2KXGΔin-AREγActin-eGFP plasmid, a fragment corresponding to the three AREs and the γActin minimal promoter was PCR amplified from ARE_3-Luciferase (Pierreux et al., 2000) and was cloned into pT2KXGΔin (Urasaki et al., 2006). The pCS2-Fgf8a plasmid was generated by PCR amplifying the *fgf8a* ORF with oligos extended with BamH1 and EcoR1 restriction sites and then cloned into pCS2+. The pGEMT-pri-miR430 and pGEMT-oep plasmids were generated by PCR amplification and cloning into pGEMT (Promega). For 3'UTR reporter assays, the pFTX4KeGFPC1-DrLft2-3'UTR plasmid was generated by PCR amplifying the *lft2*-3'UTR from a 30% epiboly zebrafish cDNA library, which was

cloned into pFTX4KeGFPC1 (Harding et al., 2014). pCS2+3xPT-miR-204 and pCS+3xPT-miR-430 were as previously described (Giraldez et al., 2005). Wild type *lft1* was PCR amplified and cloned into pCS2+. Point mutations in putative proprotein cleavage sites were introduced by PCR and plasmids were all verified by sequencing. For *in vitro* translation of Lft1/2, pCS2-lft1-gfp and pCS2-lft2-gfp were used (Muller et al., 2012). The following additional plasmids were used for mRNA injections: pXFD (XdnFgfR) (Amaya et al., 1991) (injected at a concentration of 500 pg/embryo), pCS2+ndr1 (Feldman et al., 1998) (injected at a concentration of 10 pg/embryo). mRNA was synthesized and microinjections were performed as previously described (Ramel and Hill, 2013).

Oligonucleotides used for cloning

Oligo name	**Sequence 5' – 3'**	**For plasmid**
ARE_XhoI_fw	CTTGCTCGAGGGTACCCCCCACCCTTGC	pT2KXGΔIN-AREγActin-EGFP
ARE_AgeI_rv	CTTGACCGGTCGACGGATCCCCGTCCACTG	pT2KXGΔIN-AREγActin-EGFP
fgf8a_BamH1_fw	CCGGGGATCCAACATGAGACTCATACCTTC	pCS2+-FGF8A
fgf8a_ EcoRI_rv	CCGGGAATTCTCAACGCTCTCCTGAGTAGC	pCS2+-FGF8A
pre-miR-430a_fw	CTATCGGTACCCTCACAAAGGCA	pGEMt_miR-430_ISH
pre-miR-430b_rv	CTACCCCAACTTGATAGCACTTT	pGEMt_miR-430_ISH
lft2_3UTR_fw_BamH1	TGACGGATCCCAGTGTGGTGTCGAATAGTTTGCTC	pFTX4KeGFPC1-DrLft2-3'UTR
lft2-3UTR_rv SpeI	CATGACTAGTTAAAATTAAGCTACTTACTTTATTT	pFTX4KeGFPC1-DrLft2-3'UTR
lft1_fw1_ClaI	CAGGATCCCATCGATGCCACCATGACTTC	pCS2+Lft1 + cleavage mutants
lft1_rv1_Xho1	CGCGCTCGAGCTTATACAACTGAAATATTGTCCATTGCGCATCC	pCS2+Lft1 + cleavage mutants
lft1_mut1_fw	AACTTCACCACTCA**G**GAAAACGCCGCTCGC	pCS2+lft1-mutant-C1
lft1_mut1_rv	GCGAGCGGCGTTTTC**C**TGAGTGGTGAAGTT	pCS2+lft1-mutant-C1
lft1_mut2_fw	ACACAAG**G**GCTCCATACCGGAGAG	pCS2+lft1-mutant-C2
lft1_mut2_rv	CTCTCCGGTATGGAGC**C**CTTGTG	pCS2+lft1-mutant-C2
lft1_mut3_fw	CAAAGAC**G**GTGAAATGTGCTGCAGGG	pCS2+lft1-mutant-C3
lft1_mut3_rv	CCCTGCAGCACATTTCAC**C**GTCTT	pCS2+lft1-mutant-C3

	TG	
tdgf1_fw	GAACACGCAAACGCCGCAAC	pGEMt-oep-ISH
tdgf1_rv	CACTCGAGCTACAGCAGGCGGT	pGEMt-oep-ISH

The letters in red indicate mutated residues.

Lefty antibodies and immunoblotting

Peptides CVHFTTQDPDDNTLGKPELVLYTLN and PELVLYTLDLDEYGSQGNC were used to generate rabbit antisera against Lft1 and Lft2 respectively. The antibodies were affinity purified using commercially available columns, coupled to the peptides according to the manufacturer's instructions (Thermo Scientific, 44999). For blotting of endogenous Lft1, 10 embryos were manually de-yolked without disrupting the blastoderm and snap frozen in 10 µl E3 medium. Lysates were prepared and immunoblotting was performed as previously described (Batut et al., 2007). The following additional antibodies were used: anti–phosphylated-Smad2 (Millipore, 04-953), anti-Smad2 (Cell Signaling Technology, 3103), anti-Smad3 (also detects zebrafish Smad2) (Abcam, ab28379), anti-phosphorylated-Erk (Sigma M8159), anti-Erk (Santa Cruz, sc-94), anti-GFP (Roche, 11814460001), anti-MCM6 (Santa Cruz Biotechnology, sc-9843) and anti-Actin (Sigma, A3853). All experiments were performed at least in triplicate. The quantifications of protein expression in Figure 4F were performed using ImageJ.

WISH and sectioning

Whole mount in situ hybridization (WISH) and double fluorescent WISH were performed and imaged as previously described (Ramel and Hill, 2013). For a full list of plasmids and oligos that were used to generate riboprobes, see the Tables below. All WISH experiments were performed at least in duplicate and unless stated otherwise in the figure legend, lateral views are shown with dorsal to the right. For sectioning, embryos were embedded in

paraffin, sectioned at 8 μm and counterstained with Nuclear Fast Red for 5 min (Vector laboratories, H3403). Quantification of *ta* staining in Figure 1 was performed blind and the statistical difference assessed using a Mann-Whitney U test. For expression analysis of mature *miR-430a* and *miR-430b*, locked nucleic acid (LNA) probes (Exiqon), digoxigenin (DIG) labeled as previously described (Harding et al., 2014), were used for WISH. The sequences of the probes were: *dre-miR-430a*: 5'- CTACCCCAACAAATAGCACTTA -3'; *dre-miR-430b*: 5'- CTACCCCAACTTGATAGCACTTT -3'. The hybridization temperature was optimized and found to be 55°C for both probes. To quantitate the number of *sox17*-positive cells, 75% epiboly embryos were stained by WISH for *sox17*, after which the blastoderm was dissected from the yolk and opened up along the dorsal midline to count the number of individual cells under a stereomicroscope. The statistical difference was assessed using a Mann-Whitney U test.

WISH probes generated from plasmids.

Target gene	**Plasmid**	**reference**	**Digest/ RNA polymerase**
ta	pBKS-ntl-a	(Schulte-Merker et al., 1992)	Xho1/T7
fscn1a	pBS-fscn1a	Thisse et al., 2001 ZFIN online publication	BamH1/T7
lft2	pAD-gal4-Lft2	(Bisgrove et al., 1999)	MluI/T7
ndr1	pBSK-squint	(Rebagliati et al., 1998a)	BamH1/T7
ndr2	pBSK-cyclops	(Rebagliati et al., 1998b)	Not1/T7
eGFP	pBSK-eGFP	(Narayanan et al., 2011)	BamH1/T7
pri-miR-430	pGEMt-miR-430-ISH	n/a	Not1/T7
tdgf1	pGEMt-oep-ISH	n/a	Not1/T7
smad2	pCRII-Smad2_ISH	(Dick et al., 2000)	BamH1/T7
noto/*flh*	pBSK-flh	(Talbot et al., 1995)	EcoR1/T7
sox3	pBUT2-Sox3	(Dee et al., 2008)	XbaI/T7
fgf3	pBSK-fgf3	(Kiefer et al., 1996)	BamH1/T7
fgf8a	pBSK-fgf8a (cb110)	Thisse et al., 2001 ZFIN online publication	Not1/T7
sox17	pBSK-sox17	(Alexander and Stainier, 1999)	NcoI/Sp6

gsc	pBS-gsc	(Stachel et al., 1993)	EcoR1/T7

Oligonucleotides for WISH probes generated by PCR

Oligo name	**Sequence 5' – 3'**	**RNA polymerase**
acvr1ba_fw	TCCCTCGGGTCAGCCTGGTT	T7
acvr1ba_T7_rv	TAATACGACTCACTATAGGAGGCCGAAGCCTCTG GTCACA	T7
foxh1_fw	GTCCACAGGGATGGCGCAGG	T7
foxh1_T7_rv	TAATACGACTCACTATAGGAAGCGCATGCTTGGA GGGGC	T7
lft1-ISH_fw	TGCCTCCTTTGCGCAGCACT	T7
lft1-ISH_T7_rv	TAATACGACTCACTATAGGCGGCAGCCGCCTTTA CACCT	T7

Northern blotting, ePAT and qPCR

Detection of miRNAs by northern blotting was performed as described (Harding et al., 2014) using 16 µg of total RNA and ^{32}P-radiolabeled complementary LNA probes. Detection of miRNAs by qPCR was as described (Harding et al., 2014). ePAT was performed as previously described (Janicke et al., 2012) except that for the gene-specific PCR amplification, random-primed cDNA was used. Samples were separated on 8% non-denaturing polyacrylamide gels, which were silver stained (Pierreux et al., 2000). Sequences of oligonucleotides used in these assays are listed in the Table below.

Oligonucleotides used in ePAT experiments

ePAT_Anchor	GCGAGCTCCGCGGCCGCGTTTTTTTTTTTT
ePAT_anchor _rv	AGCTCCGCGGCCGCG
ndr1_ePAT_fw	TTGCAGAATGCGGCTGCCACTGA
ndr1_GS_rv	TTACAGATAAGGCAAACACGCAAAGC
lft1_ePAT_fw	AGGAAATGCGCGGTCGTCGAG
lft1_GS_rv	ACAACAAACCCGTGCTATATGCTC
lft2_ePAT_fw	AGGATGCAAGCAGCCTAAACG
lft2_GS_rv	AAGTGCTCAGTGGGGATTTGGG

For qPCR, mRNA was extracted using Trizol (Life Technologies, 15596-026), reverse transcribed with AffinityScript (Agilent, 600559), diluted 1:20 and measured with Express Sybr Green ER (Invitrogen, 11784). Calculations were performed using the ddCT method and were normalized to levels of *eef1a1l1,* and then to the values obtained in untreated cells. Experiments were performed at least in triplicate and statistical differences were assessed using t-tests with a 95% confidence interval. All oligonucleotides used for qPCR assays are listed in the Table below.

Oligonucleotides used in qPCR experiments

Oligo name	**Sequence 5' – 3'**	**target**
eef1a1l1_fw	TGCTGTGCGTGACATGAGGCAG	*eukaryotic translation elongation factor 1 alpha 1, like 1*
eef1a1l1_rv	CCGCAACCTTTGGAACGGTGT	*eukaryotic translation elongation factor 1 alpha 1, like 1*
odc1_fw	ACACTATGACGGCTTGCACCG	*ornithine decarboxylase 1*
odc1_rv	CCCACTGACTGCACGATCTGG	*ornithine decarboxylase 1*
eGFP_fw	TTCAGCCGCTACCCCGACCA	*enhanced GFP*
eGFP_rv	ACCAGGGTGTCGCCCTCGAA	*enhanced GFP*
lft1_fw	GCTGGTGCTTTACACACTCAACCT	*lefty1*
lft1_rv	GTTCCCTGCAGCACATTTCACG	*lefty1*
lft2_fw	GGACATGGGCGCACCAGAACT	*lefty2*
lft2_rv	TACCCGGCCGGCTCGATGAT	*lefty2*
ndr1_fw	CTCCGTCTTGAGCCTCGTCG	*nodal-related 1*
ndr1_rv	TCGCTGGACGTCATCGCTTG	*nodal-related 1*
ndr2_fw	AATGCATACCGGTGCGAGGG	*nodal-related 2*
ndr2_rv	GCAGGAACACGACTGGGGTG	*nodal-related 2*
ta_fw	AAGACGCGGAGTTGTGGACC	*T, brachyury homolog a*
ta_rv	ACTGGCTCTGAGCACGGGAA	*T, brachyury homolog a*
fscn1a_fw	ACTGCCTCTACCAAGTCTGC	*fascin actin-bundling protein 1a*
fscn1a_rv	ATTTTCCATTGGTGGCACGC	*fascin actin-bundling protein 1a*
dre-miR-430a	TAAGTGCTATTTGTTGGGGTAG	*dre-miR-430a*
dre-miR-430b	AAAGTGCTATCAAGTTGGGGTAG	*dre-miR-430b*
dre-miR-430c	TAAGTGCTTCTCTTTGGGGTAG	*dre-miR-430c*
dre-miR-30d	TGTAAACATCCCCGACTGGAAG	*dre-miR-30d*
miR_universal_rv	GCGAGCACAGAATTAATACGACTCAC	*reverse for all miRNA PCRs*

gsc_fw	CAAGAGAACAACTGGCACGA	*goosecoid*
gsc_rv	TCCTCTGACGACCTTTT	*goosecoid*
noto_fw	TCTCAGGAGAACTCCAAGAGTC	*notochord homeobox*
noto_rv	GCTGCCCTTGGAACTCAGAT	*notochord homeobox*

Supplemental References

Agathon, A., Thisse, B., and Thisse, C. (2001). Morpholino knock-down of antivin1 and antivin2 upregulates nodal signaling. Genesis *30*, 178-182.

Alexander, J., and Stainier, D.Y. (1999). A molecular pathway leading to endoderm formation in zebrafish. Curr Biol *9*, 1147-1157.

Amaya, E., Musci, T.J., and Kirschner, M.W. (1991). Expression of a dominant negative mutant of the FGF receptor disrupts mesoderm formation in Xenopus embryos. Cell *66*, 257-270.

Batut, J., Howell, M., and Hill, C.S. (2007). Kinesin-mediated transport of Smad2 is required for signaling in response to TGF-β ligands. Dev Cell *12*, 261-274.

Bisgrove, B.W., Essner, J.J., and Yost, H.J. (1999). Regulation of midline development by antagonism of lefty and nodal signaling. Development *126*, 3253-3262.

Bruce, A.E., Howley, C., Dixon Fox, M., and Ho, R.K. (2005). T-box gene eomesodermin and the homeobox-containing Mix/Bix gene mtx2 regulate epiboly movements in the zebrafish. Dev Dyn *233*, 105-114.

Dee, C.T., Hirst, C.S., Shih, Y.H., Tripathi, V.B., Patient, R.K., and Scotting, P.J. (2008). Sox3 regulates both neural fate and differentiation in the zebrafish ectoderm. Dev Biol *320*, 289-301.

Dick, A., Mayr, T., Bauer, H., Meier, A., and Hammerschmidt, M. (2000). Cloning and characterization of zebrafish smad2, smad3 and smad4. Gene *246*, 69-80.

Feldman, B., Gates, M.A., Egan, E.S., Dougan, S.T., Rennebeck, G., Sirotkin, H.I., Schier, A.F., and Talbot, W.S. (1998). Zebrafish organizer development and germ-layer formation require nodal-related signals. Nature *395*, 181-185.

Giraldez, A.J., Cinalli, R.M., Glasner, M.E., Enright, A.J., Thomson, J.M., Baskerville, S., Hammond, S.M., Bartel, D.P., and Schier, A.F. (2005). MicroRNAs regulate brain morphogenesis in zebrafish. Science *308*, 833-838.

Harding, J.L., Horswell, S., Heliot, C., Armisen, J., Zimmerman, L.B., Luscombe, N.M., Miska, E.A., and Hill, C.S. (2014). Small RNA profiling of Xenopus embryos reveals novel miRNAs and a new class of small RNAs derived from intronic transposable elements. Genome Res *24*, 96-106.

Janicke, A., Vancuylenberg, J., Boag, P.R., Traven, A., and Beilharz, T.H. (2012). ePAT: a simple method to tag adenylated RNA to measure poly(A)-tail length and other 3' RACE applications. RNA *18*, 1289-1295.

Kawakami, K. (2007). Tol2: a versatile gene transfer vector in vertebrates. Genome Biol *8 Suppl 1*, S7.

Kawakami, Y., Raya, A., Raya, R.M., Rodriguez-Esteban, C., and Izpisua Belmonte, J.C. (2005). Retinoic acid signalling links left-right asymmetric patterning and bilaterally symmetric somitogenesis in the zebrafish embryo. Nature *435*, 165-171.

Kiefer, P., Mathieu, M., Mason, I., and Dickson, C. (1996). Secretion and mitogenic activity of zebrafish FGF3 reveal intermediate properties relative to mouse and Xenopus homologues. Oncogene *12*, 1503-1511.

Kimmel, C.B., Ballard, W.W., Kimmel, S.R., Ullmann, B., and Schilling, T.F. (1995). Stages of embryonic development of the zebrafish. Dev Dyn *203*, 253-310.

Maves, L., Jackman, W., and Kimmel, C.B. (2002). FGF3 and FGF8 mediate a rhombomere 4 signaling activity in the zebrafish hindbrain. Development *129*, 3825-3837.

Muller, P., Rogers, K.W., Jordan, B.M., Lee, J.S., Robson, D., Ramanathan, S., and Schier, A.F. (2012). Differential diffusivity of Nodal and Lefty underlies a reaction-diffusion patterning system. Science *336*, 721-724.

Narayanan, A., Thompson, S.A., Lee, J.J., and Lekven, A.C. (2011). A transgenic wnt8a:PAC reporter reveals biphasic regulation of vertebrate mesoderm development. Dev Dyn *240*, 898-907.

Pei, W., Noushmehr, H., Costa, J., Ouspenskaia, M.V., Elkahloun, A.G., and Feldman, B. (2007). An early requirement for maternal FoxH1 during zebrafish gastrulation. Dev Biol *310*, 10-22.

Picker, A., Roellig, D., Pourquie, O., Oates, A.C., and Brand, M. (2009). Tissue micromanipulation in zebrafish embryos. Methods Mol Biol *546*, 153-172.

Pierreux, C.E., Nicolas, F.J., and Hill, C.S. (2000). Transforming growth factor beta-independent shuttling of Smad4 between the cytoplasm and nucleus. Mol Cell Biol *20*, 9041-9054.

Ramel, M.C., and Hill, C.S. (2013). The ventral to dorsal BMP activity gradient in the early zebrafish embryo is determined by graded expression of BMP ligands. Dev Biol *378*, 170-182.

Rebagliati, M.R., Toyama, R., Fricke, C., Haffter, P., and Dawid, I.B. (1998a). Zebrafish nodal-related genes are implicated in axial patterning and establishing left-right asymmetry. Dev Biol *199*, 261-272.

Rebagliati, M.R., Toyama, R., Haffter, P., and Dawid, I.B. (1998b). cyclops encodes a nodal-related factor involved in midline signaling. Proc Natl Acad Sci U S A *95*, 9932-9937.

Schulte-Merker, S., Ho, R.K., Herrmann, B.G., and Nusslein-Volhard, C. (1992). The protein product of the zebrafish homologue of the mouse T gene is expressed in

nuclei of the germ ring and the notochord of the early embryo. Development *116*, 1021-1032.

Stachel, S.E., Grunwald, D.J., and Myers, P.Z. (1993). Lithium perturbation and goosecoid expression identify a dorsal specification pathway in the pregastrula zebrafish. Development *117*, 1261-1274.

Talbot, W.S., Trevarrow, B., Halpern, M.E., Melby, A.E., Farr, G., Postlethwait, J.H., Jowett, T., Kimmel, C.B., and Kimelman, D. (1995). A homeobox gene essential for zebrafish notochord development. Nature *378*, 150-157.

Urasaki, A., Morvan, G., and Kawakami, K. (2006). Functional dissection of the Tol2 transposable element identified the minimal cis-sequence and a highly repetitive sequence in the subterminal region essential for transposition. Genetics *174*, 639-649.

Westerfield, M. (2000). The zebrafish book. A guide for the laboratory use of zebrafish (Danio rerio), 4th Edition edn (Eugene: University of Oregon Press).